Available online at www.sciencedirect.com
SCIENCE DIRECT®
Coordination Chemistry Reviews 238–239 (2003) 55–82
COORDINATION CHEMISTRY REVIEWS
www.elsevier.com/locate/ccr

Towards a rigorously defined quantum chemical analysis of the chemical bond in donor–acceptor complexes☆

Gernot Frenking*, Karin Wichmann, Nikolaus Fröhlich, Christoph Loschen, Matthias Lein, Jan Frunzke, Víctor M. Rayón

Fachbereich Chemie der Philipps-Universität Marburg, Hans-Meerwein-Strasse, D-35042 Marburg, Germany

Received 26 April 2002; accepted 27 September 2002

Contents

Abstract

The results of an energy decomposition analysis of various classes of donor–acceptor complexes of transition metals and main-group elements are discussed. It is shown that the nature of the chemical bond can be quantitatively identified in terms of Pauli repulsion, electrostatic attraction and covalent bonding. The covalent and electrostatic contributions to the interatomic attraction can be precisely given by using a well defined partitioning method in conjunction with accurate quantum chemical calculations of the geometries and bond energies. This is shown for six classes of donor–acceptor complexes: (a) transition metal carbonyl complexes; (b) transition metal complexes with Group-13 diyl ligands ER (E = B–Tl); (c) transition metal complexes with phosphane ligands $(CO)_5TMPX_3$ (TM = Cr, Mo, W; X = H, Me, F, Cl); (d) main group complexes with phosphane ligands $X_3B–PY_3$ and $X_3Al–PY_3$ (X = H, F, Cl; Y = F, Cl, Me, CN); (e) transition metal metallocene complexes $Fe(\eta^5\text{-}E_5)_2$ and $FeCp(\eta^5\text{-}E_5)$ (E = CH, N, P, As, Sb); (f) main group metallocenes ECp_2 (E = Be–Ba, Zn, Si–Pb) and ECp (E = Li–Cs, B–Tl).

Keywords: Bonding analysis; Donor–acceptor bonds; Energy partitioning; Transition metal complexes; Main group complexes

Abbreviations: ADF, Amsterdam density functionals; HSAB, hard and soft acids and bases; VSEPR, valence shell electron pair repulsion; ZORA, zero order regular approximation; EDA, energy decomposition analysis; ETS, extended transition state; VB, valence bond; MO, molecular orbital; HF, Hartree-Fock; TZP, triple zeta plus polarization; TZ2P, triple zeta plus 2 polarization; HOMO, higher occupied molecular orbital; LUMO, lowest unoccupied molecular orbital; TM, transition metal.

☆ Theoretical studies of inorganic compounds. XXI. Part XX: J. Frunzke, M. Lein, G. Frenking, Organometallics 21 (2002) 3351.

* Corresponding author. Tel.: +49-6421-282-5563; fax: +49-6421-282-5566
E-mail address: frenking@chemie.uni-marburg.de (G. Frenking).

0010-8545/02/$ - see front matter
PII: S0010-8545(02)00285-0

1. Introduction

The understanding and the interpretation of the chemical bond in terms of covalent and electrostatic interatomic interactions is one of the most fundamental concepts in chemistry. Numerous chemical models which are based on heuristic arguments or quantum chemical approximations such as the HSAB (hard and soft acids and bases) principle [1], the VSEPR (valence shell electron pair repulsion) model [2], the conservation of orbital symmetry [3] or the frontier orbital method [4] make use of the distinction between covalent and electrostatic bonding. A related but not exactly identical dichotomy was used by Pauling in his valence bond (VB) interpretation of the chemical bond in terms of ionic and covalent bonding [5]. In his understanding a purely ionic bond is the result of 100% electrostatic attraction between charged atoms while a purely covalent bond is formed between neutral identical atoms. Chemical bonds between unequal atoms A–B have covalent and ionic contributions which enforce the attractive interactions relative to the homoatomic bonds A–A and B–B [5].

Inspection of the chemical literature shows that the discussion in terms of electrostatic (or ionic) and covalent bonding is often made without explicit analysis of the nature of the chemical bond. The arguments are frequently based on considering the electronegativities of the atoms or on calculated atomic partial charges. The use of the latter can be misleading, because partial charges give no information about the topography of the spatial distribution of the charge. The electronic charge distribution of an atom in a molecule is often very anisotropic. An atom which carries an overall positive charge may have a local area of negative charge concentration which can lead to strong charge attraction with another positively charged atom while the partial charges would deceptively predict charge repulsion. Striking examples have recently been found by us in theoretical investigations of donor–acceptor complexes $R_3E–E'R$ where E, E′ are Group-13 elements B–Tl [6]. The donor atom E′ of the Lewis base E′R has a positve partial charge but it has a lone-electron pair which yields strong electrostatic attraction with the positively charged acceptor atom E of the Lewis acid ER_3. This shows clearly that an estimate of the electrostatic contribution to a chemical bond necessitates a more detailed analysis of the interatomic interactions.

The covalent bond is also frequently a topic of controverse discussions. If the molecule has a mirror plane the molecular orbital interactions which lead to a covalent bond may come from orbitals which have σ or π symmetry. The latter orbitals are responsible for the multiple bond character [7] and thus, the question if a bond should be regarded as single, double or triple bond is often addressed by inspecting the shape and the occupation of the π orbitals or by calculated bond orders which are based on orbital overlap and occupation numbers. However, this may not give a definite answer because the choice of the partitioning method may strongly influence the result and even qualitatively different answers may be found. Recent examples of conflicting interpretations of the multiple bond character are the Fe–Ga bond in $(CO)_4Fe–GaAr^*$ and the Ga–Ga bond in $Ar^*Ga–GaAr^{*2-}$ (Ar* = bulky aryl group) [8,9]. Several theoretical papers have been published which disagree on the question if the bonds should be considered as single or triple bonds [10,11].

Covalent and electrostatic bonding are energy terms and the most straightforward methods to address the question about the size of the two contributions should be based on a plausible definition of partitioning the *interaction energy* rather than the *charge distribution* between two chemically bonded atoms or fragments. Several conditions must be fulfilled if the results of the partitioning shall be meaningful. It must be a rigorously defined energy partitioning which can be used in conjunction with any quantum chemical method. The results of the method should not significantly change with different levels of theory. The calculated numbers cannot be compared with experimental data but they should be obtained with a plausible partitioning scheme which is mathematically well defined. It should also be possible to give a physical interpretation of the terms which are calculated with the partitioning device.

A method which fulfills the above criteria is the energy partitioning scheme which is available in the program package ADF (Amsterdam density functionals) [12]. It is based on ideas presented first in 1971 by Morokuma [13] who suggested an energy partitioning procedure for Hartree-Fock (HF) calculations. A very similar energy partitioning method was introduced in 1977 by Ziegler [14] who showed that DFT calculations of interatomic interaction energies can be analyzed and interpreted in terms of physically meaningful contributions to the chemical bond. The advantage of DFT as against HF calculations is that the Kohn-Sham orbitals include correlation effects while HF orbitals do not [12]. The fundamental steps of the Morokuma/Ziegler energy partitioning are given in Section 2.

Two years ago we started a research program which has the goal to give an understanding of the chemical bond in terms of rigorously defined and physically meaningful contributions which are given by partitioning the results of accurate quantum chemical calculations. We have chosen the partitioning method of ADF because the energy terms can be identified with three main components of the chemical bond, i.e. Pauli repulsion, electrostatic attraction and covalent interaction. The latter term can be broken down into contributions which come from orbitals with different symmetry.

Thus, the calculated data may be directly used to address the question if π interactions are important in a chemical bond. The answer to the question is then given together with the information about the relative contributions of covalent and electrostatic interactions to the chemical bond. The latter term is often neglected in qualitative discussions of single versus multiple bond character. Thus, the results of the energy partitioning analysis give a comprehensive picture of the nature of the chemical bond in terms of familiar concepts of traditional bonding models. This is the goal of our research program: to build a bridge between the results of accurate quantum chemical calculations and traditional bonding models.

This paper gives a first summary of the research projects which have been finished until now. We investigated the nature of the chemical bond in donor–acceptor complexes of transition metal complexes with carbonyl ligands, Group-13 diyl ligands ER (E = B–Tl) and phosphane ligands PR_3, in sandwich complexes of transition metals and main group elements with carbocyclic and heterocyclic ligands, and in complexes between borane and alane Lewis acids with phosphane Lewis bases. The results are very promising and we plan to extend the work to other classes of compounds. We will also analyze the chemical bonding between open-shell fragments.

2. Methods

The geometries and bond energies of the complexes which shall not be discussed here have been calculated with gradient corrected DFT methods (B3LYP [15] and/or BP86 [16]) using valence basis sets of DZP or TZP quality. Details of the methods and the results can be found in the original publications which are cited below. Relativistic effects have been considered by the zero order regular approximation (ZORA) [17] which is more reliable than the widely used Pauli formalism.

The bonding interactions either between the metal fragment L'_nM and a single ligand L or between the bare metal M and the ligands L_n have been analyzed with the energy decomposition scheme of the program package ADF [12] which is based on the EDA method of Morokuma [13] and the ETS partitioning scheme of Ziegler [14]. The bonding analysis was always carried out at the BP86 level using TZP or TZ2P quality basis functions. Details are given in the cited original papers. The bond dissociation energy ΔE between two fragments A and B is partitioned into several contributions which can be identified as physically meaningful entities. First, ΔE is separated into two major components ΔE_{prep} and ΔE_{int}:

$$\Delta E = \Delta E_{prep} + \Delta E_{int} \quad (1)$$

ΔE_{prep} is the energy which is necessary to promote the fragments A and B from their equilibrium geometry and electronic ground state to the geometry and electronic state which they have in the compound AB. ΔE_{int} is the instantaneous interaction energy between the two fragments in the molecule. The latter quantity is the focus of the bonding analysis. The interaction energy ΔE_{int} can be divided into three main components:

$$\Delta E_{int} = \Delta E_{elstat} + \Delta E_{Pauli} + \Delta E_{orb} \quad (2)$$

ΔE_{elstat} gives the electrostatic interaction energy between the fragments which are calculated with a frozen electron density distribution in the geometry of the complex. ΔE_{Pauli} gives the repulsive interactions between the fragments which are caused by the fact that two electrons with the same spin cannot occupy the same region in space. The term comprises the four-electron destabilizing interactions between occupied orbitals. ΔE_{Pauli} is calculated by enforcing the Kohn-Sham determinant of AB, which results from superimposing fragments A and B, to be orthonormal through antisymmetrization and renormalisation. The stabilizing orbital interaction term ΔE_{orb} is calculated in the final step of the ETS analysis when the Kohn-Sham orbitals relax to their final form. The latter term can be further partitioned into contributions by the orbitals which belong to different irreducible representations of the point group of the interacting system.

We want to comment on the physical interpretation of the three terms given in Eq. (2). The first two terms ΔE_{elstat} and ΔE_{Pauli} are sometimes added to a single term ΔE° which is then called 'steric energy term' [18]. ΔE° can have positive or negative values and it should not be identified with the steric interaction which is often used to explain the repulsive interactions of bulky substituents. Since ΔE_{elstat} is usually attractive and ΔE_{Pauli} repulsive, the two terms often nearly cancel each other and the focus of the discussion of the bonding interactions then rests on the orbital interaction term ΔE_{orb}. This leads to the deceptive description of the bonding only in terms of orbital interactions. Because the orbital interactions can be associated with the covalent contributions to the bond and the electrostatic term with the ionic bonding the important information about the ionic/covalent character of the bond which is given by the ratio $\Delta E_{elstat}/\Delta E_{orb}$ is lost if only the sum of ΔE_{elstat} and ΔE_{Pauli} is given. We suggest that the three terms ΔE_{elstat}, ΔE_{Pauli} and ΔE_{orb} which can be identified with physical entities should be considered separately. In particular, we suggest that ΔE_{elstat} should be used to estimate the strength of the electrostatic bonding and ΔE_{orb} for the covalent bonding. Thus, the terms electrostatic and covalent bonding will always be used in this paper within our definitions of these terms. We are aware of the fact that ionic bonding is a term which originally comes from VB theory and thus, it has

conceptually a different meaning than electrostatic attraction. In the context of our analysis we are using the names ionic bonding and electrostatic attraction for the same entity, i.e. ΔE_{elstat} as defined in the energy-partitioning scheme. The reader should note that the values which are obtained for a particular bond A–B depend of course on the atomic connectivity of A and B, i.e. they are not unique for the atoms A and B.

We want to point out that our suggestion to identify ΔE_{elstat} and ΔE_{orb} with electrostatic and covalent bonding may be criticized because the former term is calculated using the frozen charge distribution of the interacting fragments. This means that the effects of charge polarization is completely adsorbed by the ΔE_{orb} term. The latter expression contains also a component which clearly does not come from covalent bonding between the fragments. It is the relaxation of the orbitals which is caused by the electrostatic effect of the other fragment. This effect becomes obvious when one fragment has orbitals which have a symmetry that the other fragment does not have. In such cases there is no orbital mixing possible and thus, no covalent interactions which come from these orbitals take place. Nevertheless, the energy levels of the occupied orbitals will change due to electrostatic effect. The associated energy change will appear as part of ΔE_{orb} and thus, it will be interpreted as covalent bonding. An example will be presented in Section 3.

We and others have thought about procedures to correct for the above mentioned problems and artefacts. A possible way to estimate polarization effects has been suggested in the original work of Kitaura and Morokuma [13b]. These authors suggested that the orbital mixing term shall be divided into intra- and interfragment contributions. This has been critisized however, because the former contribution contains always components which come from interfragment mixing because of the basis set superposition between the fragments [50]. The error will in this case even become worse when the basis set is improved because the terms do not converge to definite limits with the extension of basis sets [51]. Therefore, a further breakdown of the ΔE_{orb} term has not been considered by us. We propose to employ Eq. (2) and to use the three terms ΔE_{elstat}, ΔE_{Pauli} and ΔE_{orb} in an unmodified way because: (i) there is no undisputable way to define covelent and electrostatic bonding; (ii) the interpretation is straightforward and the three terms have a physical meaning; (iii) the terms are mathematically well defined, can be used with any quantum chemical method and they converge to definite limits with the extension of basis sets; (iv) the results appear reasonable when they are compared to previous interpretations; (v) the results indicate that there seems to be no major errors which are introduced by the fact that polarization effects are only covered by ΔE_{orb} and by the inclusion of orbital relaxation in the latter term.

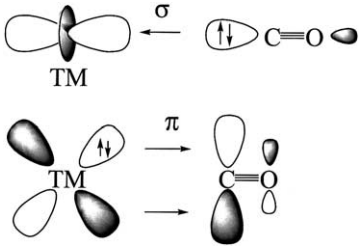

Fig. 1. Schematic representation of the synergistic OC→TM σ donation and OC←TM π backdonation.

3. Transition metal-carbonyl complexes

The chemical bonding between a transition metal and a CO ligand in carbonyl complexes is usually described in terms of donor–acceptor interactions between the occupied orbitals of the ligand and the empty orbitals of the metal and vice versa. The generally accepted bonding model which is based on the orbital interaction scheme that was first suggested by Dewar [19] is shown in Fig. 1.

The dominant contributions come from: (i) the electron donation of the CO σ HOMO which is mainly located at the carbon atom into an empty d(σ)-orbital of the metal; and (ii) the backdonation of an occupied d(π)-orbital of the metal into the empty π*-orbital of CO. Numerous theoretical studies investigated the question which of the two contributions that are shown in Fig. 1 are more important for the bonding. Most investigations analyzed the charge distribution between the metal and the ligand [20] and only few papers analyzed the contributions of the different energy terms to the metal–CO interactions [21]. Nearly all studies focused on neutral compounds [22]. There is general agreement that the TM→CO π backdonation is more important for the chemical bonding than the TM←CO σ donation.

We investigated the nature of the metal–CO bonding in the series of isoelectronic hexacarbonyls $TM(CO)_6^q$ ($TM^q = Hf^{2-}$, Ta^-, W, Re^+, Os^{2+}, Ir^{3+}) with the energy partitioning method [23]. Details about the calculated geometries and bond dissociation energies can be found in our paper and shall not be discussed here. Table 1 gives the most important results of the bonding analysis for the interactions between one CO ligand and a $TM(CO)_5^q$ fragment.

The results shown in Table 1 suggest that the contribution of the $(CO)_5TM^q \rightarrow CO$ π backdonation increases from the trication $Ir(CO)_6^{3+}$ to the dianion $Hf(CO)_6^{2-}$ while the strength of the $(CO)_5TM^q \leftarrow CO$ σ donation increases in the opposite direction. This is a

Table 1
Energy decomposition analysis of $TM(CO)_5^q + CO$ at BP86/TZP (kcal mol^{-1}) [a]

	$Hf(CO)_6^{2-}$	$Ta(CO)_6^-$	$W(CO)_6$	$Re(CO)_6^+$	$Os(CO)_6^{2+}$	$Ir(CO)_6^{3+}$
ΔE_{int}	−56.59	−51.31	−49.63	−52.74	−61.92	−78.90
ΔE_{Pauli}	76.63	100.74	118.31	126.86	125.44	115.94
ΔE_{elstat} [b]	−59.38 (44.6%)	−76.56 (50.4%)	−90.08 (53.6%)	−97.69 (54.4%)	−98.48 (52.6%)	−93.08 (47.8%)
ΔE_{orb} [b]	−73.83 (55.4%)	−75.48 (49.6%)	−77.87 (46.4%)	−81.92 (45.6%)	−88.87 (47.4%)	−101.76 (52.2%)
$\Delta E(A_1)$ [c]	−17.19 (23.3%)	−25.79 (34.3%)	−35.92 (46.1%)	−47.34 (57.8%)	−60.08 (67.6%)	−75.39 (74.2%)
$\Delta E(A_2)$	0.00	0.00	0.00	0.00	0.00	0.00
$\Delta E(B_1)$	0.05	0.02	−0.03	−0.07	−0.09	−0.10
$\Delta E(B_2)$	−0.05	−0.07	−0.07	−0.07	−0.06	−0.05
$\Delta E(E)$ [c]	−56.64 (76.7%)	−49.64 (65.8%)	−41.85 (53.8%)	−34.44 (42.1%)	−28.64 (32.2%)	−26.22 (25.8%)
ΔE_{prep}	5.75	3.05	3.65	4.38	5.00	5.16
ΔE ($= -D_e$)	−50.84	−48.26	−45.98	−48.36	−56.92	−73.74
	Distances					
TM–C	2.195	2.112	2.061	2.036	2.034	2.055

Calculated interatomic distances TM–C (Å).
[a] Values taken from Ref. [23].
[b] Values in parentheses give the percentage of attractive interactions $\Delta E_{elstat} + \Delta E_{orb}$.
[c] Values in parentheses give the percentage of orbital interactions ΔE_{orb}.

reasonable result because the energy level of the HOMO of $(CO)_5TM^q$ increases from $Ir(CO)_6^{3+}$ to $Hf(CO)_6^{2-}$ while the energy level of the LUMO of $(CO)_5TM^q$ decreases from $Hf(CO)_6^{2-}$ to $Ir(CO)_6^{3+}$. The calculations show that, in the neutral complex $W(CO)_6$, the π backdonation contributes more to the chemical bonding than the σ donation. The latter term becomes much stronger, however, in the negatively charged hexacarbonyls.

Fig. 2 shows the peculiar trend of the three energy contributions ΔE_{Pauli}, ΔE_{elstat} and ΔE_{orb} to the total interaction energy ΔE_{int}. The trend of the ΔE_{int} values has a bowl-shaped curve where the lowest binding energy is predicted for the neutral complex $W(CO)_6$ (note that the attractive energies have negative values). The ΔE_{elstat} term in $W(CO)_6$ is larger than the ΔE_{orb} term. This means that the $(CO)_5W$–CO bonding in $W(CO)_6$ is more electrostatic than covalent [52]. Which

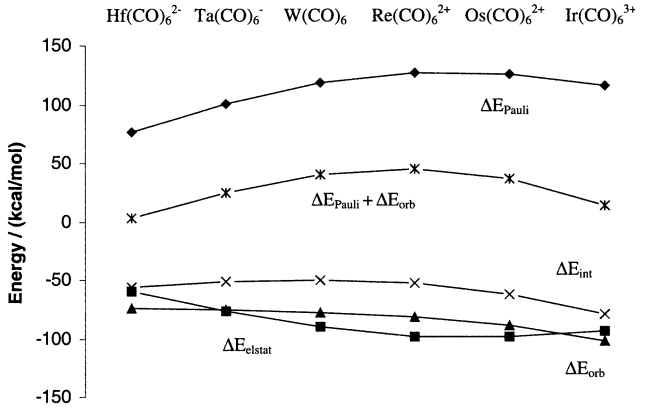

Fig. 2. Trends of the various terms of the energy decomposition analysis of $(CO)_5TM^q$–CO. Reproduced with permission from Ref. [23]. Copyright by the American Chemical Society.

factor is responsible for the increase in the binding energy from $W(CO)_6$ to $Hf(CO)_6^{2-}$? Table 1 shows that *both* attractive components of the interaction energy decrease, i.e. electrostatic and covalent bonding in $TM(CO)_6^q$ become *weaker* from $TM^q = W$ to $TM^q = Hf^{2-}$. Thus, the stronger bonding in the negatively charged hexacarbonyls does not arise from an increase of the attractive interactions but from the large decrease of the repulsive term ΔE_{Pauli}. The increase in the ΔE_{int} values from $W(CO)_6$ to $Ir(CO)_6^{3+}$, however, is mainly caused by the stronger covalent interactions which come from the large increase of the $(CO)_5TM^q \leftarrow CO$ σ donation (Table 1).

There is one surprising result which comes out of the energy analysis. Fig. 2 shows that, for the highest charged species $Hf(CO)_6^{2-}$ and $Ir(CO)_6^{3+}$, the covalent bonding is larger than the electrostatic bonding while for $W(CO)_6$, $Re(CO)_6^+$ and $Os(CO)_6^{2+}$ it holds that $\Delta E_{orb} < \Delta E_{elstat}$. This is a counterintuitive result because it means that the highest charged complexes have the smallest degree of electrostatic bonding. The explanation for this finding can be given when the energy levels of the interacting orbitals are considered. The highly charged pentacarbonyls have a very high lying HOMO ($Hf(CO)_5^{2-}$) and low lying LUMO ($Ir(CO)^{3+}$) which leads to very strong orbital interactions with the LUMO and HOMO of CO, respectively. Thus, the charge of the ionic hexacarbonyls has a larger effect on the covalent bonding through its raising or lowering the orbital energy levels than on the electrostatic interactions.

The bonding situation in $TM(CO)_6^q$ was also analyzed by us in terms of interactions between a naked TM^q metal atom and the $(CO)_6$ ligand cage. The chemical bonding in transition metal hexacarbonyls is often discussed with the help of the qualitative orbital

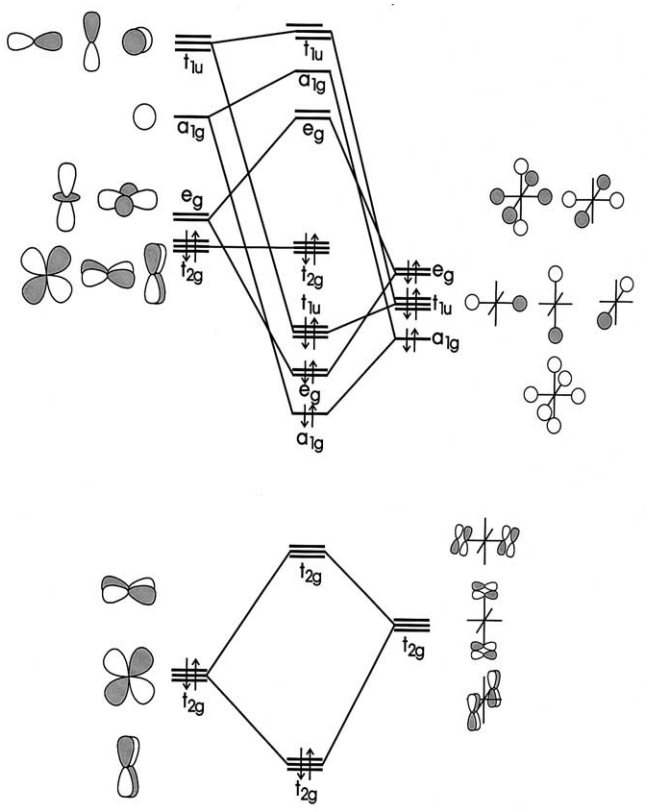

Fig. 3. Splitting of the orbital energy levels of an octahedral d^6 transition metal complex TML_6 where the ligand L has occupied donor orbitals with σ symmetry (top) and empty acceptor orbitals with π symmetry.

correlation diagram which is shown in Fig. 3 [24]. The σ donor orbitals of the six CO ligands split in an octahedral field into three sets of orbitals which have e_g, t_{1u} and a_{1g} symmetry. Fig. 3 shows that the metal

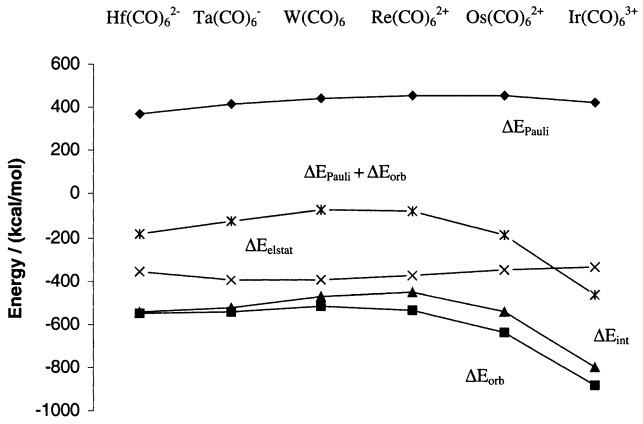

Fig. 4. Trends of the various terms of the energy decomposition analysis of TM^q–$(CO)_6$ at BP86/TZP. Reproduced with permission from Ref. [23]. Copyright by the American Chemical Society.

acceptor orbitals are the s AO (a_{1g}), p AOs (t_{1u}) and the e_g set of d AOs. The remaining set ot (t_{2g}) d AOs of a d^6 TM is occupied and serves as donor orbital for the TM→$(CO)_6$ π backdonation. The advantage of the octahedral ligand field is that the contributions of the e_g, t_{1u} and a_{1g} orbitals to the TM←$(CO)_6$ σ donation shows directly the relative importance of the metal valence orbitals to the metal ligand bonding. There has been a controversial discussion about the question whether the empty metal p AOs should be considered as true valence orbitals or as polarization functions [25].

Table 2 gives the results of the energy decomposition analysis of TM^q–$(CO)_6$. The trend of the three components ΔE_{Pauli}, ΔE_{elstat} and ΔE_{orb} is shown in Fig. 4. Please note that the covalent term ΔE_{orb} follows closely the trend of the total interaction energy ΔE_{int}, except that ΔE_{int} decreases but ΔE_{orb} increases from $W(CO)_6$ to

Table 2
Energy decomposition analysis of $TM^q+(CO)_6$ at BP86/TZP (kcal mol^{-1}) [a]

	$Hf(CO)_6^{2-}$	$Ta(CO)_6^-$	$W(CO)_6$	$Re(CO)_6^+$	$Os(CO)_6^{2+}$	$Ir(CO)_6^{3+}$
ΔE_{int}	−543.90	−525.56	−473.89	−456.57	−544.40	−801.58
ΔE_{Pauli}	367.40	413.38	438.80	454.51	451.33	420.93
ΔE_{elstat} [b]	−358.62 (39.4%)	−397.62 (42.3%)	−396.24 (43.4%)	−375.09 (41.2%)	−353.44 (35.5%)	−337.81 (27.6%)
ΔE_{orb} [b]	−552.68 (60.6%)	−541.32 (57.7%)	−516.44 (56.6%)	−536.00 (58.8%)	−642.27 (64.5%)	−884.70 (72.4%)
$\Delta E(A_{1g})$ [c]	−9.48 (1.7%)	−10.49 (1.8%)	−15.40 (2.8%)	−27.42 (4.6%)	−47.63 (6.4%)	−78.78 (7.5%)
$\Delta E(A_{2g})$	0.00	0.00	0.00	0.00	0.00	0.00
$\Delta E(E_g)$ [c]	−83.36 (14.6%)	−113.07 (20.3%)	−159.08 (29.3%)	−233.72 (39.6%)	−348.84 (46.9%)	−520.66 (49.5%)
$\Delta E(T_{1g})$ [c]	−1.30 (0.3%)	−0.98 (0.2%)	−2.88 (0.5%)	−8.91 (1.5%)	−19.41 (2.6%)	−33.92 (3.2%)
$\Delta E(T_{2g})$ [c]	−437.42 (76.6%)	−397.59 (71.2%)	−308.18 (56.8%)	−200.33 (34.0%)	−101.14 (13.6%)	−43.82 (4.2%)
$\Delta E(A_{1u})$	−0.03	−0.04	−0.03	0.00	−0.02	−0.02
$\Delta E(E_u)$	0.00	−0.00	0.00	0.00	0.00	0.00
$\Delta E(T_{2u})$ [c]	−2.74 (4.8%)	−2.00 (0.4%)	−4.35 (0.8%)	−11.60 (2.0%)	−23.86 (3.2%)	−40.17 (3.8%)
$\Delta E(T_{1u})$ [c]	−18.35 (3.2%)	−17.15 (3.1%)	−26.52 (4.9%)	−54.00 (9.2%)	−101.37 (13.6%)	−167.33 (15.9%)
$\Delta E(T_{1u}(\sigma))$	−12.97	−12.06	−18.65	−38.53	−73.98	−125.68
$\Delta E(T_{1u}(\pi))$	−5.38	−5.09	−7.87	−15.47	−27.39	−41.65

[a] Taken from Ref. [23].
[b] Values in parentheses give the percentage of attractive interactions $\Delta E_{elstat}+\Delta E_{orb}$.
[c] Values in parentheses give the percentage of orbital interactions ΔE_{orb}.

$Re(CO)_6^+$. The nature of the bonding becomes less electrostatic when one goes from neutral $W(CO)_6$ towards the highest charged complexes $Hf(CO)_6^{2-}$ and $Ir(CO)_6^{3+}$. The explanation for this paradoxical result has been given above.

The most important results come from the breakdown of the orbital term into the contributions by the orbitals which have different symmetry. The contribution of the t_{2g} orbitals which gives the TM → $(CO)_6$ π backdonation is rather small in the trication $Ir(CO)_6^{3+}$ but it becomes stronger when the metal is less positively charged and it is the dominant orbital term in the neutral and negatively charged hexacarbonyls. The e_g orbitals make clearly the largest contribution to the TM ← $(CO)_6$ σ donation. The e_g term is always much larger than the t_{1u} and a_{1g} terms. Table 2 gives also energy contributions by t_{1g} and t_{2u} orbitals which are not shown in Fig. 3. Fig. 5 shows schematically all orbitals which contribute to ΔE_{orb}. The t_{1g} and t_{2u} orbitals are occupied ligand orbitals. The relaxation of the ligand orbital in the final step of the energy partitioning analysis lowers the energy of the molecule. Thus, part of the stabilization energy which comes from the orbital term is not related to the metal–ligand bonding. Fig. 5 shows also that the t_{1u} term does not only give the TM ← $(CO)_6$ σ donation into the p(σ) AO but part of the t_{1u} stabilization energy comes from the TM ← $(CO)_6$ π donation of the occupied π orbitals of CO into the empty p(π) AO of the metal. In order to estimate the σ and π contributions to the t_{1u} term, we used the size of the overlaps of the metal p orbitals with the σ and π orbitals of $(CO)_6$. Table 2 shows that the π contribution to the t_{1u} term is always much less than the σ contribution.

Concerning the question whether the metal p orbitals should be considered as valence orbitals or polarization function, the results in Table 2 show that the contribution of the t_{1u} term (metal p orbitals) is always larger than the a_{1g} term (metal s-orbital). Thus, the p orbitals are as important as the s orbitals for the bonding in these compounds and thus, must be considered as valence functions.

4. Transition metal complexes with Group-13 diyl ligands ER (E = B–Tl)

Unlike the TM–CO bonding in carbonyl complexes which was undisputed in the literature, the nature of the donor–acceptor interactions between a transition metal and a Group-13 diyl ligand ER (E = B–Tl) has been controversially discussed for several years. The first complex with a ligand ER which was characterized by X-ray structure analysis was $(CO)_4Fe$–AlCp* [26]. The Fe–Al bond was interpreted in terms of σ donation and π backdonation between the interacting ligand and metal fragment which is shown in Fig. 6.

Two questions have been in the center of the discussion. One question concerns the strength of the TM → ER π backdonation. The formally empty p(π) AO of atom E may receive electronic charge from the occupied π orbitals of the substituent R or from the metal (Fig. 6). Because the first examples of stable complexes with ligands ER had strong π donor substituents such as Cp* [26] and NR_2 [27] it was supposed that TM → ER π backdonation is rather weak [28]. The synthesis of the stable complex $(CO)_4Fe$–GaAr* where Ar* is a bulky aryl substituent which is a poor π donor substituent let the author suggest that there is strong Fe → Ga π backdonation and that the compound would have a Fe≡Ga triple bond [8]. This view was soon challenged by other workers who analyzed the charge distribution in model compounds of $(CO)_4Fe$–GaAr*

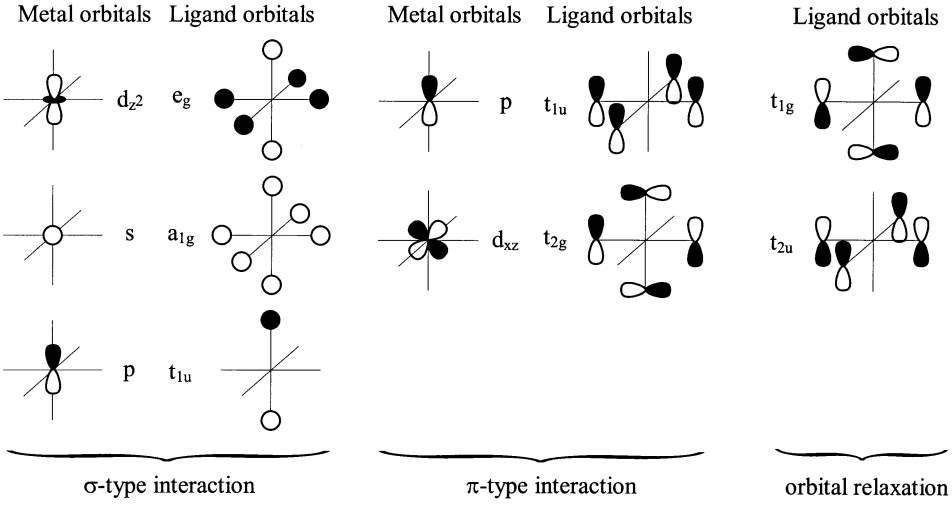

Fig. 5. Graphical representation of the orbital interaction terms of the energy decomposition analysis of TM^q–$(CO)_6$ given in Table 2.

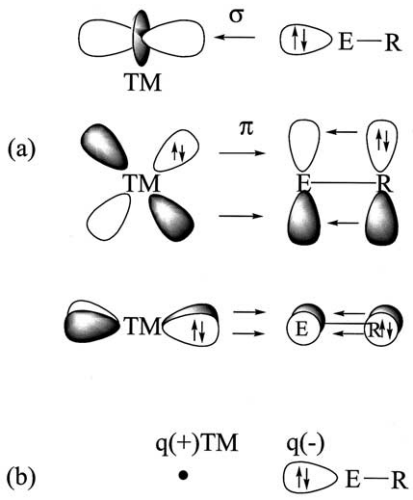

Fig. 6. (a) Schematic representation of the TM–ER orbital interactions when R has occupied p(π) orbitals. (b) Schematic representation of the dominant electrostatic interactions between the local electronic charge concentration at the donor atom E and the nucleus of the acceptor atom Fe. Note that the donor atom E has an overall positive partial charge and the TM atom an overall negative partial charge.

with less bulky aryl groups which indicated that there may only be a bond order of ca. 1 [10a].

The second controversial question was about the relative contributions of electrostatic and covalent bonding in the Group-13 diyl complexes. The results of population analyses of complexes with a TM–ER bond showed that the Group-13 atom E is always highly positively charged while the TM atom carries a large negative charge [10b,10c,26,29]. This led to the conclusion that the Fe–ER bond has a substantial ionic character. The calculated partial charges were misleading, however, because the dominant charge attraction takes place between the negative charge concentration of the σ donor lone-pair orbital of the Lewis base ER and the positively charged nucleus of TM. This is schematically shown in Fig. 6. Thus, a meaningful insight into the bonding situation in the complexes could only be given if the actual electronic charge distribution would become a subject of an energy partitioning analysis [30]. This has been done by us in two recent papers where we analyzed the bonding situation in $(CO)_4Fe–ER$, $Fe(EMe)_5$ and $TM(EMe)_4$ (R = Cp, $N(SiH_3)_2$, Ph, Me; TM = Ni, Pd, Pt) [31,49]. The most important conclusions are now summarized.

We begin our discussion with the results for the series $(CO)_4Fe–ECp$ (E = B–Tl) which are shown in Table 3. We give only the data for the axial isomers of the compounds because the equatorial isomers except for E = In were slightly higher in energy than the axial species and because the energy partitioning analysis of the equatorial isomers gave very similar results [31a]. Fig. 7 shows the trend of the energy contributions ΔE_{Pauli}, ΔE_{elstat} and ΔE_{orb} for E = B–Tl.

The most important results of the complexes $(CO)_4Fe–ECp$ can be summarized as follows. The Fe–B bond between iron and the lightest Group-13 element boron has a significantly higher electrostatic (61.6%) than covalent character (38.4%). The covalent contributions to the Fe–E bonds increase for the heavier Group-13 elements E where it becomes as large as the electrostatic contribution. The covalent bonding comes mainly from the Fe←ECp σ donation. The contribution of the Fe→ECp π backdonation is much smaller, i.e. $<20\%$ of the total ΔE_{orb} term.

Fig. 7 shows nicely that the values of ΔE_{Pauli}, ΔE_{elstat} and ΔE_{orb} for $(CO)_4Fe–ECp$ run parallel from E = B–

Table 3
Energy decomposition analysis of the axial isomers of $Fe(CO)_4–ECp$ and $Fe(CO)_5$ at BP86/TZP (kcal mol^{-1}) [a]

	BCp	AlCp	GaCp	InCp	TlCp	CO
ΔE_{int}	−90.3	−65.2	−31.7	−27.1	−33.1	−54.6
ΔE_{Pauli}	211.6	154.3	69.8	63.6	64.1	134.8
ΔE_{elstat} [b]	−186.0 (61.6%)	−112.1 (51.1%)	−47.1 (46.6%)	−40.0 (44.1%)	−42.7 (44.0%)	−98.0 (51.7%)
ΔE_{orb} [b]	−115.9 (38.4%)	−107.4 (48.9%)	−54.4 (53.4%)	−50.7 (55.9%)	−54.2 (56.0%)	−91.4 (48.3%)
ΔE_{σ} [c]	−93.8 (80.9%)	−92.3 (85.9%)	−47.2 (86.8%)	−45.3 (89.3%)	−48.9 (89.4%)	−47.6 (52.1%)
ΔE_{π} [c]	−22.1 (19.1%)	−15.1 (14.1%)	−7.2 (13.2%)	−5.4 (10.7%)	−5.8 (10.6%)	−43.8 (47.9%)
ΔE_{prep}	15.0	12.5	8.7	7.3	19.5	8.1
ΔE ($= -D_e$)	−75.3	−52.7	−23.0	−19.8	−13.6	−46.5
Atomic partial charges						
q(Fe)	−0.56	−0.58	−0.51	−0.49	−0.45	–
q(E)	0.32	1.18	0.96	1.06	0.89	–
	Distances					
Fe–E	1.968	2.253	2.395	2.548	2.578	–

Atomic partial charges q and calculated bond distances Fe–E (Å).
[a] Values taken from Ref. [31a].
[b] Values in parentheses give the percentage contribution to the total attractive interactions $\Delta E_{elstat} + \Delta E_{orb}$.
[c] Values in parentheses give the percentage contribution to the total orbital interactions ΔE_{orb}.

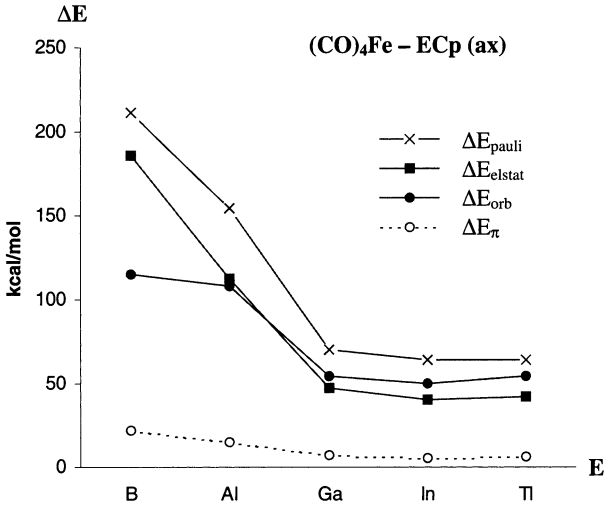

Fig. 7. Trends of the absolute values of the Pauli repulsion ΔE_{Pauli}, electrostatic interactions ΔE_{elstat}, total orbital interactions ΔE_{orb} and π-orbital interactions ΔE_{π} to the Fe–E bonding interactions in the axial isomers of $(CO)_4$Fe–ECp at BP86/TZP. Reproduced with permission from Ref. [31a]. Copyright by the American Chemical Society.

Tl except for the ΔE_{orb} value of the boron complex. There is a steep increase of ΔE_{Pauli} and ΔE_{elstat} from Al to B while the ΔE_{orb} value remains nearly the same. The larger values for ΔE_{Pauli} and ΔE_{elstat} for the boron complex can be explained with the much shorter Fe–B distance compared to Fe–Al which leads to stronger overlap repulsion between the occupied orbitals of the ligand and the metal fragment (ΔE_{Pauli}) and to stronger attraction between the Fe nucleus and the electron lone pair of the donor ligand (ΔE_{elstat}, see Fig. 6b) but why is there hardly any change in the ΔE_{orb} value? The explanation can be given when the nature of the dominant orbital interaction is analyzed. Table 3 shows that the dominant contribution of ΔE_{orb} comes from the Fe ← ECp σ donation. Fig. 6a displays the shape of the interacting orbitals. The σ donor orbital of E at first overlaps in a bonding fashion with the lope of the d_{z^2}-orbital of Fe, which has the same sign. At shorter distances, there is an overlap with the tubular-shaped lope of the d_{z^2}-orbital which has an opposite sign, thus leading to antibonding orbital interactions. This cancels the increase of the bonding orbital interactions which therefore remains nearly constant. The electrostatic interactions do not depend on the sign of the orbitals.

Table 3 gives also the atomic partial charges of the complexes which have been calculated with the NBO method [32]. The charges suggest that: (i) there is charge attraction between the positively charged atoms E and the negatively charged Fe; (ii) the charge attraction of the Fe–B bond should be significantly weaker compared to the Fe–E bonds of the heavier atoms E. The energy analysis reveals that and why both conclusions are wrong.

Table 3 gives also the results of the energy partitioning analysis of the Fe–CO(ax) bond of $Fe(CO)_5$. What is the difference between the nature of the Fe–ECp and Fe–CO bonds? The data show that the ratio between electrostatic to covalent bonding of the two ligands is quite similar. A significant difference, however, is found when the contributions by the Fe → L π backdonation for L = CO and ECp are compared. The calculated values show that CO is a strong π acceptor ligand while ECp is not.

In order to examine the statement that the Fe → ER π backdonation becomes a significant part of the orbital interactions when the substituent R is a weak π donor such as an aryl group [8] we carried out an energy partitioning analysis of $(CO)_4$Fe–EPh (Ph = phenyl) [31a]. The results are given in Table 4. The trend of the energy contributions is displayed in Fig. 8.

The calculations show that the interaction energies ΔE_{int} and bond dissociation energies D_e of the $(CO)_4$Fe–EPh complexes are larger than those of the $(CO)_4$Fe–ECp molecules. A comparison of the calculated energy contributions of the axial Fe–EPh bonds (Table 4) with those of the Fe–ECp bonds (Table 3) reveals that the nature of the bonding with regard to the ratio of covalent and electrostatic bonding is very similar to each other. This becomes obvious when the trends of ΔE_{elstat} and ΔE_{orb} in the two sets of molecules are compared (Figs. 7 and 8). The ΔE_{orb} boron value in the $(CO)_4$Fe–EPh exhibits a similar anomaly as for the $(CO)_4$Fe–ECp compounds. The crucial information, however, concerns the degree of π bonding to the ΔE_{orb} term. Table 4 shows that the contribution of ΔE_{π} to the covalent bonding in the series $(CO)_4$Fe–EPh is indeed larger than in $(CO)_4$Fe–ECp. However, Fe–E π bonding remains much smaller than σ bonding in the former complexes. The largest contribution is found in the boron complex $(CO)_4$Fe–BPh where ΔE_{π} is 33.4% of the total covalent term. The value for ΔE_{π} in $(CO)_4$Fe–GaPh is only 17.2% of ΔE_{orb} (Table 4). It follows that the iron–gallium bond in in $(CO)_4$Fe–GaAr* should not be considered as a triple bond. The stronger and shorter Fe–E bonds in the $(CO)_4$Fe–EPh complexes are caused by several factors of which enhanced π bonding is only a minor component.

Table 4 shows also the results of the energy analysis of the equatorial isomers of $(CO)_4$Fe–EPh. The calculated data show that the Fe–EPh bonding interactions in the axial and equatorial isomers are very similar. However, the latter isomers have C_{2v} symmetry while the axial form have only C_s symmetry. Thus, the calculated energy values of the orbitals having different symmetry can be used to distinguish between the in-plane (b_1) and out-of-plane (b_2) contributions to the Fe–EPh π bonding. The results show that the in-plane contributions are as expected larger than the out-of-plane values but the latter are not negligible.

Table 4
Energy decomposition analysis of the axial and equatorial isomers of $Fe(CO)_4$–EPh at BP86/TZP (kcal mol^{-1}) [a]

	BPh		AlPh		GaPh		InPh		TlPh	
	ax	eq	ax	eq	ax	eq	ax	eq	ax	eq
ΔE_{int}	−110.3	−109.8	−73.2	−71.1	−61.0	−55.5	−48.8	−48.7	−49.4	−42.9
ΔE_{Pauli}	276.6	319.2	173.8	192.3	129.5	130.0	112.3	112.2	98.7	96.4
ΔE_{elstat} [c]	−230.4 (59.6%)	−258.8 (60.3%)	−127.3 (51.5%)	−147.6 (56.0%)	−102.3 (53.7%)	−107.5 (58.0%)	−87.0 (54.0%)	−91.7 (57.0%)	−79.3 (53.5%)	−81.3 (58.6%)
ΔE_{orb} [c]	−156.5 (40.4%)	−170.2 (39.7%)	−119.7 (48.5%)	−115.8 (44.0%)	−88.2 (46.3%)	−76.0 (42.0%)	−74.1 (46.0%)	−69.2 (43.0%)	−68.8 (46.5%)	−58.0 (41.4%)
ΔE_{σ} [d]	−104.3 (66.6%)	−110.3 (64.8%)	−98.2 (82.0%)	−91.6 (79.1%)	−73.0 (82.8%)	−61.7 (79.1%)	−63.4 (85.6%)	−57.7 (83.4%)	−59.8 (86.9%)	−48.6 (83.8%)
ΔE_{π} [d]	−52.2 (33.4%)	−59.9 (35.2%)	−21.5 (18.0%)	−24.2 (20.9%)	−15.2 (17.2%)	−16.3 (20.9%)	−10.7 (14.4%)	−11.5 (16.6%)	−9.0 (13.1%)	−9.4 (16.2%)
$\Delta E_{\pi\ (b1)}$ [b]	–	−39.3	–	−15.6	–	−11.4	–	−8.2	–	−6.7
$\Delta E_{\pi\ (b2)}$ [b]	–	−20.7	–	−8.6	–	−4.9	–	−3.3	–	−2.7
ΔE_{prep}	10.1	10.8	9.4	8.2	8.7	6.1	8.1	5.2	8.6	4.9
$\Delta E\ (=-D_e)$	−100.2	−99.0	−63.8	−62.9	−52.3	−49.4	−40.7	−43.5	−40.8	−38.0
	Distances									
TM–E	1.803	1.800	2.217	2.206	2.296	2.304	2.478	2.488	2.478	2.544

Calculated interatomic distances TM–E (Å).

[a] Values Taken from Ref. [31a].

[b] π (b1)-orbital is in the Ph plane and π (b2)-orbital is perpendicular to the Ph plane.

[c] Values in parentheses give the percentage of the attractive interactions $\Delta E_{elstat} + \Delta E_{orb}$.

[d] Values in parentheses give the percentage contribution to the total orbital interactions ΔE_{orb}.

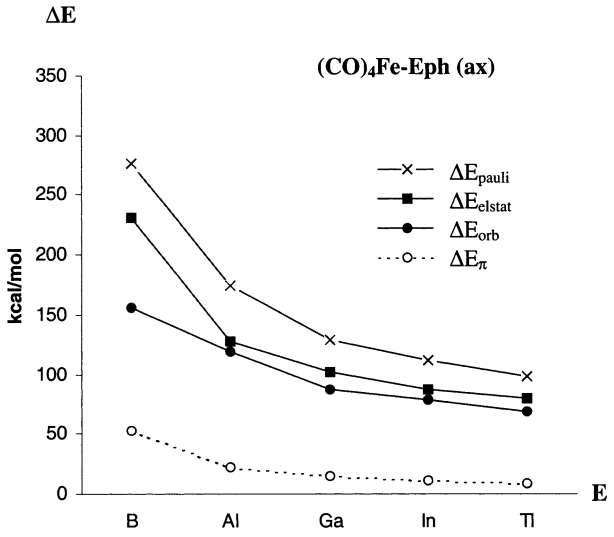

Fig. 8. Trends of the absolute values of the Pauli repulsion ΔE_{Pauli}, electrostatic interactions ΔE_{elstat}, total orbital interactions ΔE_{orb} and π-orbital interactions ΔE_{π} to the Fe–E bonding interactions in the axial isomers of $(CO)_4$Fe–EPh at BP86/TZP. Reproduced with permission from Ref. [31a]. Copyright by the American Chemical Society.

We analyzed also the Fe–E bonding in $(CO)_4$Fe–ER with the strong π donor $R = N(SiH_3)_2$ and the weak π donor $R = CH_3$ [31a]. The results of the former compounds are very similar to those of $(CO)_4$Fe–ECp and thus, are not discussed here while the results of $(CO)_4$Fe–EMe are given in Table 5 [33]. The results are very similar to those of $(CO)_4$Fe–EPh (Table). The reason why we show the values for $(CO)_4$Fe–EMe is that we found substantially different results when we analyzed the metal–ligand bonding in the homoleptic complexes $Fe(EMe)_5$ and $TM(EMe)_4$ ($Me = CH_3$; TM = Ni, Pd, Pt) [31]. The results of $Fe(EMe)_5$ are shown in Table 6. The data of $TM(EMe)_4$ and $TM(CO)_4$ are given in Table 7. The trends of the energy terms ΔE_{elstat}, ΔE_{orb} and ΔE_{Pauli} in $Fe(EMe)_5$ and $Ni(EMe)_4$ are displayed in Figs. 9 and 10.

A comparison of the bonding analysis of the homoleptic complexes $Fe(EMe)_5$ (Table 6) with the results of the heteroleptic species $(CO)_4$FeEMe (Table 5) shows that the BDEs of the former are higher than those of the latter. What is the reason for the increase in the bond energies? The calculations shows that the higher bond strength of the homoleptic species is caused by the intrinsic interactions energies ΔE_{int} which are significantly larger than those of the heteroleptic molecules. Further breakdown of the ΔE_{int} term into the attractive forces shows that, in $Fe(EMe)_5$, the electrostatic interactions contribute more to the chemical bonding than in $(CO)_4$FeEMe. Another difference between the homopletic and heteroleptic species is the relative contibution of the π backdonation. Table 6 shows that the Fe→ER π backdonation in $Fe(EMe)_5$ is between 32 and 46% of the ΔE_{orb} term which means that it contributes significantly to the covalent bonding. The conclusion is that Fe→ER π backdonation is weaker than Fe→CO π backdonation. In $(CO)_4$FeER, the two forces compete and therefore, Fe→ER π backdonation is weak. In homoleptic complexes $Fe(EMe)_5$ there is no competition and therefore, Fe→ER π backdonation becomes quite strong.

Table 7 shows that the statement concerning significant Fe→ER π backdonation holds also true for other transition metals. In $TM(EMe)_4$ (TM = Ni, Pd, Pt), the contribution of TM→EMe π backdonation is between 33 and 49% of the covalent term ΔE_{orb}. However, the bonding interactions in the Group-14 complexes $TM(EMe)_4$ is mainly electrostatic. The ΔE_{elstat} term contributes between 75 and 65% of the total attractive interactions. Table 7 gives also the results for the tetracarbonyls $TM(CO)_4$. The covalent bonding in the latter is larger than in the $TM(EMe)_4$ compounds but it remains smaller than the electrostatic bonding. Another difference between the two sets of compounds is the strength of the TM→L π backdonation which is larger for L = CO than for L = EMe. The most important difference between the tetracarbonyls and the tetradiyl complexes is the total bond energy. Table 7 shows that the BDE of the TM–CO bond is always less than the BDE of the weakest TM–EMe bond, i.e. the TM–TlMe bond. This is the reason why $Ni(CO)_4$ but not $Pd(CO)_4$ and $Pt(CO)_4$ are stable complexes at room temperature while the tetradiyl species of the heavier Group-14 elements can be isolated [31b]. Figs. 9 and 10 show that the trends of the bonding contributions ΔE_{Pauli}, ΔE_{elstat} and ΔE_{orb} and also the ΔE_{π} term in $Fe(EMe)_5$ and $Ni(EMe)_4$ are very similar. The 'boron effect' of the heteroleptic complexes $(CO)_4$FeER is much weaker in the homoleptic species.

5. Transition metal complexes with phosphane ligands $(CO)_5TMPX_3$ (TM = Cr, Mo, W; X = H, Me, F, Cl)

The interpretation of the chemical bonding in TM phosphane complexes in terms of donor–acceptor interactions focuses often on the strength of the TM→PR_3 π backdonation [34]. Numerous theoretical and experimental studies have been carried out in order to analyze the nature of the TM–PR_3 bond [34]. Different methods have been used to estimate the π acceptor strength of different phosphanes PR_3 but the results led to controversial discussions particularly with regard to PCl_3. The interpretation of IR data of phosphane complexes by means of the Cotton–Kraihanzel force-field technique [35] led to the order of π acceptance $PF_3 > PCl_3 > P(OR)_3 > PR_3$ [36]. The interpretation of experimental NMR chemical shifts of $(CO)_nMo(PR_3)_{6-n}$ ($n = 3$–5) and a reexamination of the various

Table 5
Energy decomposition analysis of the axial and equatorial isomers of $Fe(CO)_4$–ECH_3 at BP86/TZP (kcal mol^{-1}) [c]

	BCH_3		$AlCH_3$		$GaCH_3$		$InCH_3$		$TlCH_3$	
	ax	eq	ax	eq	ax	eq	ax	eq	ax	eq
E_{int}	−110.0	−108.8	−74.4	−72.9	−62.0	−56.7	−56.3	−50.8	−51.2	−51.6
ΔE_{Pauli}	274.2	322.4	178.9	201.6	133.4	138.7	119.1	120.6	104.8	103.6
ΔE_{elstat}	−228.2	−258.8	−131.5	−153.9	−106.1	−114.0	−93.7	−99.0	−83.2	−85.7
ΔE_{orb} [a]	−156.0 (40.6%)	−172.4 (40.0%)	−121.8 (48.1%)	−120.6 (43.9%)	−89.3 (45.7%)	−81.4 (41.7%)	−81.7 (46.6%)	−72.4 (42.2%)	−72.8 (46.6%)	−69.5 (44.8%)
ΔE_{σ}	−105.5	−127.8	−101.0	−101.9	−75.0	−71.1	−71.4	−65.3	−64.3	−75.1
ΔE_{π} [b]	−50.5 (32.4%)	−44.6 (25.9%)	−20.8 (17.1%)	−18.7 (15.5%)	−14.3 (16.0%)	−10.3 (12.7%)	−10.3 (12.6%)	−7.1 (9.8%)	−8.5 (11.7%)	5.6 (6.9%)
ΔE_{prep}	10.0	10.7	9.0	8.3	8.2	5.9	7.9	5.3	5.4	5.2
$\Delta E\ (=-D_e)$	−100.0	−98.1	−65.4	−64.6	−53.8	−50.8	−48.4	−45.5	−45.8	−46.4

[a] The value in parentheses gives the percentage contribution to the total attractive interactions reflecting the covalent character of the bond.
[b] The value in parentheses gives the percentage contribution to the total orbital interactions ΔE_{orb}.
[c] Taken from Ref. [31a].

Table 6
Energy decomposition analysis of the equatorial Fe–E bonds of the complexes $Fe(ECH_3)_5$ at BP86/TZP (kcal mol^{-1}) [a]

	BCH_3	$AlCH_3$	$GaCH_3$	$InCH_3$	$TlCH_3$
ΔE_{int}	−119.2	−87.0	−67.0	−59.5	−54.1
ΔE_{Pauli}	247.8	140.2	120.8	113.9	113.0
ΔE_{elstat} [b]	−228.4 (62.2%)	−135.4 (59.6%)	−115.2 (61.3%)	−107.8 (62.2%)	−103.8 (62.1%)
ΔE_{orb} [b]	−138.6 (37.8%)	−91.8 (40.4%)	−72.6 (38.7%)	−65.6 (37.8%)	−63.3 (37.9%)
ΔE_{σ} [c]	−74.6 (53.8%)	−55.0 (59.9%)	−45.5 (62.7%)	−41.7 (63.6%)	−42.9 (67.8%)
ΔE_{π} [c]	−64.0 (46.2%)	−36.8 (40.1%)	−27.1 (37.3%)	−23.9 (36.4%)	−20.4 (32.2%)
ΔE_{prep}	13.6	7.8	2.9	2.1	1.1
ΔE ($= -D_e$)	−105.6	−79.2	−64.1	−57.4	−53.1
	Distances				
TM–E	1.772	2.174	2.255	2.434	2.474

Calculated interatomic distances TM–E (Å).
[a] Values taken from Ref. [31a].
[b] Values in parentheses give the percentage of attractive interactions $\Delta E_{elstat} + \Delta E_{orb}$.
[c] Values in parentheses give the percentage contribution to the total orbital interactions ΔE_{orb}.

Table 7
ETS analysis of the TM–L bonds in $TM(EMe)_4$ and $TM(CO)_4$ (TM = Ni, Pd, Pt; E = B–Tl) at BP86/TZP (kcal mol^{-1}) [c]

	$Ni(BMe)_4$	$Ni(AlMe)_4$	$Ni(GaMe)_4$	$Ni(InMe)_4$	$Ni(TlMe)_4$	$Ni(CO)_4$
ΔE_{int}	−95.44	−66.16	−57.03	−49.80	−39.42	−39.49
ΔE_{Pauli}	236.24	140.08	130.87	113.45	94.34	122.97
ΔE_{elstat}	−215.47	−132.74	−123.70	−108.53	−89.18	−96.57
ΔE_{orb} [a]	−116.21 (35.0%)	−73.50 (35.6%)	−64.20 (34.2%)	−54.72 (33.5%)	−44.58 (33.3%)	−65.89 (40.6%)
ΔE_{σ}	−59.85	−44.87	−38.91	−33.40	−26.88	−30.60
ΔE_{π} [b]	−56.35 (48.5%)	−28.63 (39.0%)	−25.29 (39.4%)	−21.32 (39.0%)	−17.70 (39.7%)	−35.29 (53.6%)
ΔE_{prep}	3.30	1.26	3.62	3.14	4.13	10.64
ΔE ($= -D_e$)	−92.14	−64.9	−53.41	−46.66	−35.29	−28.85
	$Pd(BMe)_4$	$Pd(AlMe)_4$	$Pd(GaMe)_4$	$Pd(InMe)_4$	$Pd(TlMe)_4$	$Pd(CO)_4$
ΔE_{int}	−80.51	−56.09	−46.66	−40.69	−30.37	−25.57
ΔE_{Pauli}	280.59	169.64	154.28	131.74	110.65	126.61
ΔE_{elstat}	−248.46	−162.61	−144.96	−127.64	−105.54	−94.68
ΔE_{orb} [a]	−112.64 (31.2%)	−63.12 (28.0%)	−55.98 (27.9%)	−44.79 (26.0%)	−35.48 (25.2%)	−57.50 (37.8%)
ΔE_{σ}	−60.21	−38.32	−34.01	−27.99	−22.64	−29.68
ΔE_{π} [b]	−52.42 (46.5%)	−24.80 (39.3%)	−21.97 (39.2%)	−16.80 (37.5%)	−12.84 (36.2%)	−27.82 (48.4%)
ΔE_{prep}	6.61	2.35	4.65	3.89	4.70	12.76
ΔE ($= -D_e$)	−73.90	−53.74	−42.01	−36.80	−25.67	−12.81
	$Pt(BMe)_4$	$Pt(AlMe)_4$	$Pt(GaMe)_4$	$Pt(InMe)_4$	$Pt(TlMe)_4$	$Pt(CO)_4$
ΔE_{int}	−96.89	−67.09	−57.71	−49.74	−38.10	−35.37
ΔE_{Pauli}	362.43	220.38	203.98	174.79	149.55	194.47
ΔE_{elstat}	−316.47	−206.93	−187.09	−164.47	−137.75	−140.34
ΔE_{orb} [a]	−142.85 (31.1%)	−80.54 (28.0%)	−74.60 (28.5%)	−60.06 (26.8%)	−49.90 (26.6%)	−89.50 (38.9%)
ΔE_{σ}	−80.33	−51.94	−48.24	−39.82	−33.66	−49.19
ΔE_{π} [b]	−62.51 (43.8%)	−28.60 (35.5%)	−26.36 (35.3%)	−20.24 (33.7%)	−16.24 (32.5%)	−40.31 (45.0%)
ΔE_{prep}	9.18	4.12	7.40	6.52	7.86	20.71
ΔE ($= -D_e$)	−87.71	−62.97	−50.31	−43.22	−30.24	−14.66

[a] The value in parentheses gives the percentage contribution to the total attractive interactions reflecting the covalent character of the bond.
[b] The value in parentheses gives the percentage contribution to the total orbital interactions, ΔE_{orb}.
[c] Taken from Ref. [31b].

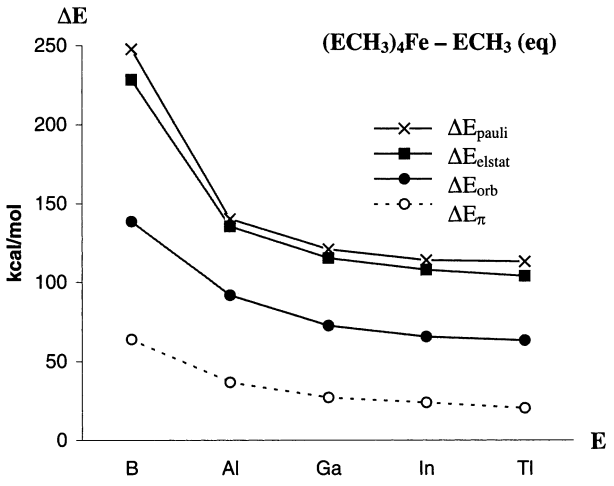

Fig. 9. Trends of the absolute values of the Pauli repulsion ΔE_{Pauli}, electrostatic interactions ΔE_{elstat}, total orbital interactions ΔE_{orb} and π-orbital interactions ΔE_{π} to the Fe–E bonding interactions in the equatorial isomers of $(ECH_3)_4Fe–ECH_3$ at BP86/TZP. Reproduced with permission from Ref. [31a]. Copyright by the American Chemical Society.

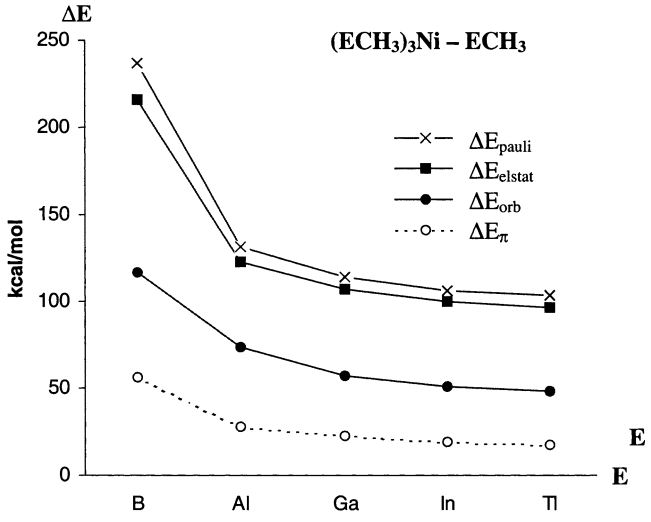

Fig. 10. Trends of the absolute values of the Pauli repulsion ΔE_{Pauli}, electrostatic interactions ΔE_{elstat}, total orbital interactions ΔE_{orb} and π-orbital interactions ΔE_{π} to the Fe–E bonding interactions in $(ECH_3)_3Ni–ECH_3$ at BP86/TZP. Reproduced with permission from Ref. [31a]. Copyright by the American Chemical Society.

parameters used to evaluate σ and π contributions to the TM–P bond led to the suggestion that PCl_3 should be a weak π acceptor [34c,34d]. However, a subsequent theoretical study of ^{95}Mo- and ^{31}P-NMR chemical shifts indicated that PCl_3 is actually a very strong π acceptor which should be stronger than PF_3 and particularly PH_3 and PMe_3 [37]. The conflicting suggestions illustrate the dilemma which is often found when one tries to examine the nature of a chemical bond by correlating a particular property with specific components of the bonding interactions. Such an approach can be misleading because the starting point of the analysis is an *assumption* which may not be correct. Molecular properties are always the result of the simultaneous effect of the different forces in the molecule. They all need to be estimated in a well defined way before a conclusion about the strength of a particular force can be drawn.

The nature of the TM–PR_3 bond has recently been examined by us [38] and by others [39] with the energy decomposition analysis. The molecules which were calculated by us are $(CO)_5TMPX_3$ (TM = Cr, Mo, W; X = H, Me, F, Cl) [38]. The results of the energy analysis are shown in Table 8 [40].

The breakdown of the TM–P interaction energies into the contributions of ΔE_{elstat}, ΔE_{orb} and ΔE_{Pauli} shows that the repulsive term ΔE_{Pauli} has always the largest absolute values. For the TM–PH_3 and TM–PMe_3 bonds, the largest attractive contributions come from ΔE_{elstat}. The bonding in the PH_3 and PMe_3 complexes has between 56 and 65% electrostatic character. Thus, any discussion of the bonding in these molecules in terms of covalent bonding neglects the dominant part of the attractive interactions! The covalent contributions become somewhat larger in the halophosphane complexes $(CO)_5TMPF_3$ and $(CO)_5TMPCl_3$ where the electrostatic and covalent forces have nearly the same strength (Table 8). This is one difference between the TM–PX_3 (X = F, Cl) bonds and the TM–PX_3 (X = H, Me) bonds. The second difference concerns the degree of π contributions to ΔE_{orb}. Table 8 shows that π bonding in the TM–PH_3 bonds (31–34%) and particularly in the TM–PMe_3 bonds (26–28%) is clearly weaker than σ bonding, while the σ and π contributions in the TM–PF_3 and TM–PCl_3 bonds have about equal strength. The latter result answers once and for all the question about the strength of the π contributions in PCl_3 complexes. The ligand PCl_3 is as strong as π acceptor than PF_3! However, the interaction energies ΔE_{int} and the bond dissociation energies D_e show clearly (Table 8) that PCl_3 is weaker bonded than PF_3.

Fig. 11 exhibits the trend of ΔE_{int} and the energy contributions ΔE_{elstat}, ΔE_{orb} and ΔE_{Pauli} to the W–PX_3 bonds. The π contribution to ΔE_{orb} is also given. The trends of the chromium and molybdenum complexes are nearly the same and thus, they are not shown here. The most important conclusion is that the trend of the electrostatic term ΔE_{elstat} shows a much better agreement with the total interaction energy ΔE_{int} than the orbital term ΔE_{orb}. In particular, the trend of the π bonding values ΔE_{π} is very different from the curve of ΔE_{int}. The best correlation is actually found between ΔE_{int} and ΔE_{elstat}. Note that the stronger bonding of the PMe_3 ligand compared with the other other PX_3 phosphane comes clearly from the larger ΔE_{elstat} values and not from ΔE_{orb} (Table 8). The weaker bonds of the PCl_3 ligands compared with the TM–PF_3 bonds is also mainly caused by the weaker electrostatic attraction. Only the relative values of ΔE_{int} and ΔE_{elstat} for PH_3 and PF_3 do not agree with each other. Nevertheless, the

Table 8
Energy decomposition analysis of $TM(CO)_5PX_3$ at BP/TZP (kcal mol^{-1}) [c]

	$Cr(CO)_5PH_3$	$Mo(CO)_5PH_3$	$W(CO)_5PH_3$
ΔE_{int}	−33.65	−31.80	−36.38
ΔE_{Pauli}	81.53	70.71	83.66
ΔE_{elstat}	−64.86 (56.3%) [a]	−59.44 (58.0%) [a]	−71.50 (59.6%) [a]
ΔE_{orb}	−50.32 (43.7%) [a]	−43.07 (42.0%) [a]	−48.54 (40.4%) [a]
$\Delta E(A')$	−42.49	−35.69	−40.69
$\Delta E(A'')$	−7.84	−7.39	−7.86
ΔE_σ	−34.64 (68.8%) [b]	−28.30 (65.7%) [b]	−32.83 (67.6%) [b]
ΔE_π	−15.69 (31.2%) [b]	−14.78 (34.3%) [b]	−15.72 (32.4%) [b]
ΔE_{prep}	1.21	0.80	2.41
ΔE ($= -D_e$)	−32.44	−31.00	−33.97
	$Cr(CO)_5PMe_3$	$Mo(CO)_5PMe_3$	$W(CO)_5PMe_3$
ΔE_{int}	−43.66	−40.86	−46.37
ΔE_{Pauli}	96.53	85.62	99.28
ΔE_{elstat}	−85.08 (60.7%) [a]	−80.69 (63.8%) [a]	−94.85 (65.1%) [a]
ΔE_{orb}	−55.11 (39.3%) [a]	−45.79 (36.2%) [a]	−50.80 (34.9%) [a]
$\Delta E(A')$	−48.03	−39.46	−44.04
$\Delta E(A'')$	−7.08	−6.33	−6.76
ΔE_σ	−40.96 (74.3%) [b]	−33.13 (72.3%) [b]	−37.27 (73.4%) [b]
ΔE_π	−14.15 (25.7%) [b]	−12.66 (27.7%) [b]	−13.53 (26.6%) [b]
ΔE_{prep}	2.48	3.01	2.55
ΔE ($= -D_e$)	−41.18	−37.85	−43.82
	$Cr(CO)_5PF_3$	$Mo(CO)_5PF_3$	$W(CO)_5PF_3$
ΔE_{int}	−35.12	−33.51	−38.56
ΔE_{Pauli}	91.96	82.28	97.00
ΔE_{elstat}	−62.85 (49.5%) [a]	−57.43 (49.6%) [a]	−70.16 (51.8%) [a]
ΔE_{orb}	−64.24 (50.5%) [a]	−58.35 (50.4%) [a]	−65.40 (48.2%) [a]
$\Delta E(A')$	−48.45	−43.07	−48.87
$\Delta E(A'')$	−15.79	−15.29	−16.53
ΔE_σ	−32.66 (50.8%) [b]	−27.77 (47.6%) [b]	−32.35 (49.5%) [b]
ΔE_π	−31.58 (49.2%) [b]	−30.59 (52.4%) [b]	−33.05 (50.5%) [b]
ΔE_{prep}	1.34	2.66	3.14
ΔE ($= -D_e$)	−33.78	−30.85	−35.42
	$Cr(CO)_5PCl_3$	$Mo(CO)_5PCl_3$	$W(CO)_5PCl_3$
ΔE_{int}	−27.75	−26.14	−31.05
ΔE_{Pauli}	78.40	70.14	83.29
ΔE_{elstat}	−49.56 (46.7%) [a]	−45.31 (47.3%) [a]	−55.82 (48.8%) [a]
ΔE_{orb}	−56.59 (53.3%) [a]	−50.98 (52.9%) [a]	−58.51 (51.2%) [a]
$\Delta E(A')$	−43.51	−38.61	−44.86
$\Delta E(A'')$	−13.08	−12.37	−13.65
ΔE_σ	−30.43 (53.7%) [b]	−26.25 (51.5%) [b]	−31.20 (53.3%) [b]
ΔE_π	−26.16 (46.3%) [b]	−24.73 (48.5%) [b]	−27.31 (46.7%) [b]
ΔE_{prep}	1.00	2.48	2.45
ΔE ($= -D_e$)	−26.75	−23.66	−28.60

[a] Percentage of the total attractive interactions $\Delta E_{elstat} + \Delta E_{orb}$.
[b] Percentage of the total orbital interactions ΔE_{orb}.
[c] Taken from Ref. [38].

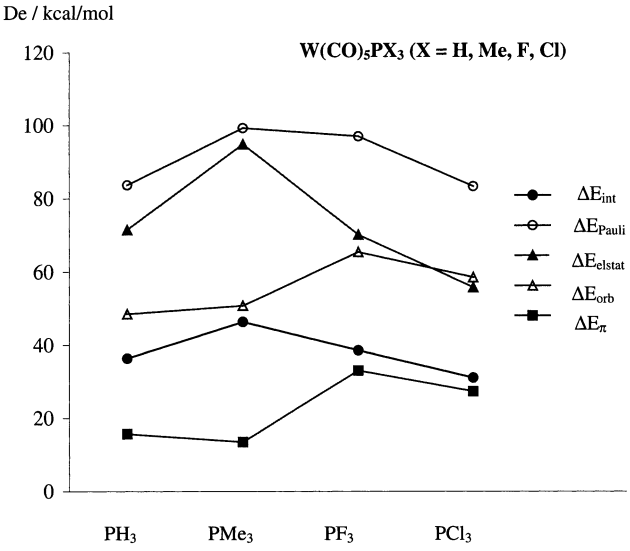

Fig. 11. Trends of the absolute values of the interaction energies ΔE_{int} and the energy contributions ΔE_{Pauli}, ΔE_{elstat}, total orbital interactions ΔE_{orb} and π-orbital interactions ΔE_π to the W–PX_3 bonds of $W(CO)_5PX_3$ at BP86/TZP. Reproduced with permission from Ref. [38]. Copyright by the American Chemical Society.

results of the energy analysis [38] suggest that the changes of the metal–phosphane bond strength is largely determined by the electrostatic interactions and not by the covalent interactions. Thus, focusing on the strength of π backdonation in phosphane complexes can be misleading!

6. Main group complexes with phosphane ligands X_3B–PY_3 and X_3Al–PY_3 (X = H, F, Cl; Y = F, Cl, Me, CN)

The chemical bonds of phosphanes as Lewis bases was also investigated by us in complexes with main

group Lewis acids of aluminum and boron. To this end we calculated the structures and bond energies of the alane and borane complexes $X_3B–PY_3$ and $X_3Al–PY_3$ (X = H, F, Cl; Y = F, Cl, Me, CN) [41] The Lewis base $P(CN)_3$ was of particular interest because, until today, there is no stable complex of $P(CN)_3$ known. Part of the theoretical work was to find out if $P(CN)_3$ is a particularly weak Lewis base, and if so, what is the reason for this. We also wanted to provide a quantitative analysis of the chemical bond in the important class of borane and alane complexes with phosphane ligands. Another focus of the work was the controversy about the reason why BCl_3 is a stronger Lewis acid than BF_3 in strongly bonded complexes. A recent reinterpretation of the bonding situation in BF_3 suggested that the boron-fluorine bonding is essentially ionic and that the intrinsic Lewis acid strength of borontrifluoride is as strong as that of BCl_3 [42]. The higher bond energies of BF_3 complexes with strong Lewis bases compared to BCl_3 was explained with the deformation energy of the BF_3 moiety which would be larger than for BCl_3. A third topic of interest was the difference between complexes of alane and borane Lewis acids.

The results of the energy partitioning analysis of the borane complexes are given in Table 9. The data of the alane complexes are listed in Table 10.

The calculated energy contributions to the donor–acceptor bonds provided a wealth of information about the nature of the bonds. Table 9 shows that the phosphane ligands PF_3, PCl_3 and $P(CN)_3$ form moderately strong bonds with BH_3 but not with BF_3 and BCl_3. The optimized structure of $Cl_3B–PF_3$ and $Cl_3B–PCl_3$ are only kinetically bonded species which dissociate into the molecular fragments after overcoming a small activation barrier [41]. The optimized structures of $F_3B–PF_3$, $F_3B–PCl_3$, $F_3B–P(CN)_3$ and $Cl_3B–P(CN)_3$ are van der Waals complexes which have very low bond dissociation energies [41]. An energy partitioning analysis of such weakly bonded species at the equilibrium geometry is not meaningful. We decided to analyze the interactions between the borane Lewis acid and the phosphane Lewis base at a standard B–P bond distance of 1.9 Å in order to find out which forces are mainly responsible for the repulsive potential in the bonding region.

The nature of the B–P bonds in the more strongly bonded complexes $H_3B–PF_3$, $H_3B–PCl_3$ and $H_3B–P(CN)_3$ is very similar. The bonds are ca. one-third electrostatic and ca. two-third covalent (Table 9). The covalent bonding comes from ca. 75% σ bonding and ca. 25% π bonding. Note that the electrostatic contribution to the B–P bonding increases when the bonds become stronger, i.e. $H_3B–PF_3 > H_3B–PCl_3 > H_3B–P(CN)_3$.

The borane complexes with the Lewis base PMe_3 have clearly different energy values than the other borane

Table 9
Energy decomposition analysis of the boron complexes $X_3B–PY_3$ at BP86/TZP (kcal mol^{-1}) [e]

	$H_3B–PF_3$	$F_3B–PF_3$ [c]	$Cl_3B–PF_3$
ΔE_{int}	−35.8	−6.2	−9.0
ΔE_{Pauli}	128.2	158.2	157.5
ΔE_{elstat}	−59.0 (36.0%) [a]	−72.8 (44.3%)	−73.0 (43.8%) [a]
ΔE_{orb}	−104.9 (64.0%) [a]	−91.5 (55.6%)	−93.5 (56.2%) [a]
ΔE_σ (A_1)	−78.4 (74.7%) [b]	−75.6 (82.7%)	−74.4 (79.6%) [b]
ΔE (A_2)	0.0 (−)	−0.1 (0.1%)	−0.1 (0.1%) [b]
ΔE_π (E_1)	−26.6 (25.3%) [b]	−15.8 (17.2%)	−19.0 (20.3%) [b]
ΔE_{prep}	8.2 (8.2+0.0) [d]	23.6 (19.7+3.9) [d]	16.2 (13.3+2.9) [d]
ΔE (= $-D_e$)	−27.5	17.4	7.3
	$H_3B–PCl_3$	$F_3B–PCl_3$ [c]	$Cl_3B–PCl_3$
ΔE_{int}	−30.3	−8.4	−7.8
ΔE_{Pauli}	112.1	149.9	105.8
ΔE_{elstat}	−48.8 (34.2%) [a]	−66.1 (41.7%)	−48.3 (42.5%) [a]
ΔE_{orb}	−93.7 (65.8%) [a]	−92.3 (58.2%)	−65.3 (57.5%) [a]
ΔE_σ (A_1)	−73.0 (77.9%) [b]	−78.6 (85.3%)	−53.9 (82.5%) [b]
ΔE (A_2)	0.0 (−)	−0.1 (0.1%)	−0.1 (0.1%) [b]
ΔE_π (E_1)	−20.7 (22.1%) [b]	−13.5 (14.6%)	−11.4 (17.4%) [b]
ΔE_{prep}	8.5 (7.1+1.4) [d]	26.1 (21.9+4.2) [d]	13.1 (11.0+2.1) [d]
ΔE (= $-D_e$)	−21.8	17.7	5.4
	$H_3B–P(Me)_3$	$F_3B–P(Me)_3$	$Cl_3B–P(Me)_3$
ΔE_{int}	−55.5	−45.4	−53.9
ΔE_{Pauli}	130.4	119.1	201.8
ΔE_{elstat}	−80.7 (43.4%) [a]	−84.1 (51.1%) [a]	−123.5 (48.3%) [a]
ΔE_{orb}	−105.2 (56.6%) [a]	−80.5 (48.9%) [a]	−132.2 (51.7%) [a]
ΔE_σ (A_1)	−91.6 (87.1%) [b]	−72.6 (90.2%) [b]	−119.4 (90.2%) [b]
ΔE (A_2)	0.0 (−) [b]	−0.2 (0.3%) [b]	−0.2 (0.2%) [b]
ΔE_π (E_1)	−13.6 (12.9%) [b]	−7.7 (9.5%) [b]	−12.6 (9.6%) [b]
ΔE_{prep}	15.7 (13.2+2.5) [d]	31.1 (26.1+5.0) [d]	31.6 (25.5+6.1) [d]
ΔE (= $-D_e$)	−39.8	−14.3	−22.4
	$H_3B–P(CN)_3$	$F_3B–P(CN)_3$ [c]	$Cl_3B–P(CN)_3$ [c]
ΔE_{int}	−26.9	1.9	−3.8
ΔE_{Pauli}	112.2	149.4	207.1
ΔE_{elstat}	−43.9 (31.5%) [a]	−55.5 (37.6%)	−85.1 (40.3%)
ΔE_{orb}	−95.3 (68.5%) [a]	−92.0 (62.3%)	−125.9 (59.6%)
ΔE_σ (A_1)	−71.6 (75.2%) [b]	−76.5 (83.2%)	−97.8 (77.7%)
ΔE (A_2)	0.0 (−)	−0.1 (0.1%)	−0.2 (0.1%)
ΔE_π (E_1)	−23.7 (24.8%) [b]	−15.4 (16.7%)	−28.0 (22.2%)
ΔE_{prep}	7.4 (6.8+0.6) [d]	21.2 (19.3+1.9) [d]	17.3 (15.3+2.0) [d]
ΔE (= $-D_e$)	−19.6	23.1	13.4

[a] Percentage of the total attractive interactions $\Delta E_{elstat} + \Delta E_{orb}$.
[b] Percentage of the total orbital interactions ΔE_{orb}.
[c] Calculated with a fixed bond length $r(B–P) = 1.90$ Å.
[d] The values in parentheses give the preparation energies of the Lewis acid and base.
[e] Taken from Ref. [41].

Table 10
Energy decomposition analysis of the aluminum complexes $X_3Al–PY_3$ at BP86/TZP (kcal mol^{-1}) [d]

	$H_3Al–PF_3$	$F_3Al–PF_3$	$Cl_3Al–PF_3$
ΔE_{int}	−8.5	−10.9	−8.9
ΔE_{Pauli}	34.8	25.3	47.9
ΔE_{elstat}	−18.3 (42.2%) [a]	−14.7 (40.7%) [a]	−25.7 (45.2%) [a]
ΔE_{orb}	−25.1 (57.8%) [a]	−21.4 (59.3%) [a]	−31.1 (54.7%) [a]
ΔE_σ (A_1)	−17.5 (69.7%) [b]	−17.9 (83.7%) [b]	−27.7 (76.4%) [b]
ΔE (A_2)	0.0 (−)	0.0 (0.1%) [b]	0.0 (0.1%) [b]
ΔE_π (E_1)	−7.6 (30.3%) [b]	−3.5 (16.3%) [b]	−7.3 (23.6%) [b]
ΔE_{prep}	1.3 (0.4+0.9) [c]	4.0 (1.9+2.1) [c]	4.2 (2.4+1.8) [c]
ΔE ($=-D_e$)	−7.2	−6.9	−4.7
	$H_3Al–PCl_3$	$F_3Al–PCl_3$	$Cl_3Al–PCl_3$
ΔE_{int}	−8.3	−12.3	−10.3
ΔE_{Pauli}	31.9	29.4	40.8
ΔE_{elstat}	−15.9 (39.4%) [a]	−15.7 (37.6%) [a]	−21.3 (41.7%) [a]
ΔE_{orb}	−24.3 (60.6%) [a]	−26.0 (62.4%) [a]	−29.8 (58.3%) [a]
ΔE_σ (A_1)	−18.3 (75.1%) [b]	−22.2 (85.4%) [b]	−24.2 (81.2%) [b]
ΔE (A_2)	0.0 (−)	0.0 (0.2%)	0.0 (0.1%) [b]
ΔE_π (E_1)	−6.1 (24.9%) [b]	−3.8 (14.5%) [b]	−5.6 (18.7%) [b]
ΔE_{prep}	1.6 (0.6+1.0) [c]	5.1 (2.7+2.4) [c]	4.7 (2.7+2.0) [c]
ΔE ($=-D_e$)	−6.7	−7.3	−5.6
	$H_3Al–P(Me)_3$	$F_3Al–P(Me)_3$	$Cl_3Al–P(Me)_3$
ΔE_{int}	−30.8	−44.8	−45.3
ΔE_{Pauli}	57.2	54.9	80.3
ΔE_{elstat}	−51.6 (58.6%) [a]	−60.6 (60.8%) [a]	−74.2 (59.0%) [a]
ΔE_{orb}	−36.4 (41.4%) [a]	−39.1 (39.2%) [a]	−51.5 (41.0%) [a]
ΔE_σ (A_1)	−31.0 (85.2%) [b]	−33.7 (86.2%) [b]	−44.4 (86.3%) [b]
ΔE (A_2)	0.0 (0.1%) [b]	−0.1 (0.4%) [b]	−0.2 (0.3%) [b]
ΔE_π (E_1)	−5.4 (14.7%) [b]	−5.2 (13.4%) [b]	−6.9 (13.4%) [b]
ΔE_{prep}	6.6 (4.4+2.2) [c]	12.4 (8.6+3.8) [c]	14.4 (9.6+4.8) [c]
ΔE ($=-D_e$)	−24.2	−32.4	−30.9
	$H_3Al–P(CN)_3$	$F_3Al–P(CN)_3$	$Cl_3Al–P(CN)_3$
ΔE_{int}	−4.7	−4.3	−2.9
ΔE_{Pauli}	30.6	23.9	36.2
ΔE_{elstat}	−11.5 (32.7%) [a]	−6.9 (24.5%)	−13.3 (34.0%) [a]
ΔE_{orb}	−23.8 (67.3%) [a]	−21.3 (75.5%) [a]	−25.8 (66.0%) [a]
ΔE_σ (A_1)	−16.1 (67.9%) [b]	−17.6 (82.4%) [b]	−19.0 (73.5%) [b]
ΔE (A_2)	0.00 (−)	0.0 (0.2%)	0.0 (0.1%) [b]
ΔE_π (E_1)	−7.6 (32.1%) [b]	−3.7 (17.4%) [b]	−6.8 (26.4%) [b]
ΔE_{prep}	0.5 (0.0+0.5) [c]	1.8 (0.8+1.0) [c]	1.6 (0.9+0.7) [c]
ΔE ($=-D_e$)	−4.2	−2.5	−1.3

[a] Percentage of the total attractive interactions $\Delta E_{elstat}+\Delta E_{orb}$.
[b] Percentage of the total orbital interactions ΔE_{orb}.
[c] The values in parentheses give the preparation energies of the Lewis acid and base.
[d] Taken from Ref. [41].

adducts. All three compounds are predicted to have moderate to strong bonds. Note that the interaction energy of $Cl_3B–PMe_3$ (−53.9 kcal mol^{-1}) is nearly as large as for $H_3B–PMe_3$ (−55.5 kcal mol^{-1}). The lower bond dissociation energy of the former compound comes from the significantly larger preparation energy ΔE_{prep}, but *not* from the intrinsic bond strength. The distortion energy of the fragments of $Cl_3B–PMe_3$ (31.6 kcal mol^{-1}) is higher than for $H_3B–PMe_3$ (15.7 kcal mol^{-1}). The electrostatic contribution to the $X_3B–PMe_3$ bonding is clearly larger than in the $X_3B–PY_3$ (Y = F, Cl, CN) complexes. The covalent bonding in the former species has even less π contribution than in the latter molecules. Another important result comes from the comparison of the data for $F_3B–PMe_3$ with $Cl_3B–PMe_3$ (Table 9). The calculations show that the lower bond dissociation energy of $F_3B–PMe_3$ (D_e = 14.3 kcal mol^{-1}) compared with $Cl_3B–PMe_3$ (D_e = 22.4 kcal mol^{-1}) does *not* come from the larger preparation energy ΔE_{prep} but is rather caused by the intrinsic interaction energy ΔE_{int}. It has recently been suggested that BF_3 is actually a stronger Lewis acid than BCl_3 and that the lower bond energies of BF_3 complexes compared to BCl_3 complexes come from the larger deformation energies of the former [42]. The results in Table 9 show that this explanation is not valid.

The energy data of the alane complexes in Table 10 show that PMe_3 forms also the strongest bonds with the AlX_3 Lewis acids but there are significant differences between the Al–P and B–P bonds. The $X_3Al–PMe_3$ bonds have a still higher electrostatic character than the $X_3B–PMe_3$ bonds which explains why $F_3Al–PMe_3$ and $Cl_3Al–PMe_3$ have stronger bonds than $H_3Al–PMe_3$. The ca. 40% contribution of the covalent Al–P bonding has mainly σ character. The main difference between the alane and borane complexes is that covalent bonding is much more important for B–P bonds than for Al–P bonds. Therefore, BH_3 is a strong Lewis acid but AlH_3 is not. Substitution of hydrogen by halogen in AlX_3 enhances the electrostatic bonding and thus, AlF_3 and $AlCl_3$ form stronger donor–acceptor bonds with PY_3 than AlH_3. The complexes $X_3Al–P(CN)_3$ are an exception because the weak bonding is caused by van der Waals interactions. Please note that the weak bonding is actually the net result of medium-sized attractive covalent and electrostatic contributions which together give 40–50 kcal mol^{-1} attraction while there is 30–40 kcal mol^{-1} Pauli repulsion.

The differences between the borane and alane complexes become obvious when the trends of the calculated bond energies D_e for $X_3B–PY_3$ are compared with $X_3Al–PY_3$ which are shown in Figs. 12 and 13. There is a strong decrease of the bond energies of the borane complexes from $H_3B–PY_3$ to $F_3B–PY_3$ while there is an increase from $H_3Al–PY_3$ to $F_3Al–PY_3$. The calculated energy contributions to the donor–acceptor bond give an explanation for this finding which is based on a well defined quantum chemical analysis of the interatomic interactions rather than heuristic assumptions.

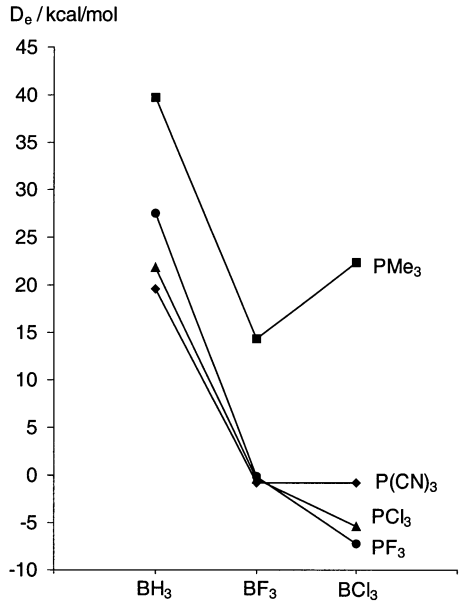

Fig. 12. Trend of the calculated bond dissociation energies D_e of the borane complexes $X_3B–PY_3$ at BP86/TZP.

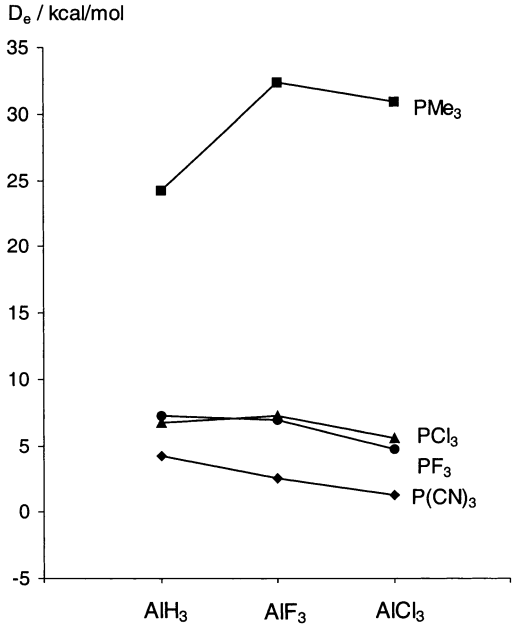

Fig. 13. Trend of the calculated bond dissociation energies D_e of the alane complexes $X_3Al–PY_3$ at BP86/TZP.

7. Transition metal metallocene complexes $Fe(\eta^5\text{-}E_5)_2$ and $FeCp(\eta^5\text{-}E_5)$ (E = CH, N, P, As, Sb)

We recently analyzed the metal ligand bonds in ferrocene ($FeCp_2$) and in the isoelectronic all-nitrogen analogue iron bispentazole $Fe(\eta^5\text{-}N_5)_2$ which has not yet been synthesized [43]. In a subsequent paper we extended the investigations to the Group-15 elements $Fe(\eta^5\text{-}E_5)_2$ and the 'semiheterocyclic' species $FeCp(\eta^5\text{-}N_5)$ (E = N–Sb) [44].

Fig. 14 shows the orbital correlation diagram for ferrocene and related molecules which is found in many textbooks of inorganic and organometallic chemistry [24,45]. Note that the metal–ligand bonding in $FeCp_2$ is usually discussed in terms of interactions between Fe^{2+} and $(Cp^-)_2$ because the Cp ligand in the complex has aromatic character which means that the π orbitals are occupied with six electrons. The neutral Cp ligand has five π electrons and thus, it is subject to Jahn-Teller distortion. It is often conceptually much easier to discuss the bonding in TM complexes between closed-shell fragments rather than open-shell species. However, one should be aware that the driving force for the metal–ligand bonding in ferrocene comes from the attractive interactions between neutral Fe and $(Cp)_2$. The bonding analysis between Fe^{2+} and $(Cp^-)_2$ is useful as an ordering scheme which may be used for comparison with other complexes which have the same bonding situation.

Table 11 gives the results of the energy decomposition analysis of $FeCp_2$ and $FeCp(\eta^5\text{-}N_5)$ between Fe^{2+} which has a $(a_{1g})^2(e_{2g})^4(e_{1g})^0$ configuration and Cp^- [43]. The calculations suggest that the attractive interactions in ferrocene which come from electrostatic forces (−598.0 kcal mol^{-1}) and covalent bonding (−567.5 kcal mol^{-1}) have about the same strength. This means that the $Fe^{2+}–(Cp^-)_2$ bonds are about half electrostatic and half covalent. Note that the repulsive contribution by the exchange term ΔE_{Pauli} (272.2 kcal mol^{-1}) is significantly smaller than the ΔE_{elstat} and ΔE_{orb} contributions. We want to remind the reader that the results of the neutral and charged hexacarbonyls $TM^q–(CO)_6$ which have been discussed above showed that the interactions between charged fragments do not necessarily have to be more electrostatic than the interactions between neutral fragments. The positive or negative charge of a fragment lowers or raises the energy levels of the occupied and vacant orbitals which yields stronger orbital interactions and thus, stronger covalent bonding.

Table 11 gives also the contributions of the orbitals with different symmetry to ΔE_{orb}. Qualitative MO arguments led to the conclusion that the electron donation from the occupied e_{1g} of $(Cp^-)_2$ into the vacant $d(e_{1g})$ AOs of Fe^{2+} (Fig. 14) should be the most important orbital term [24]. Table 11 shows that the e_{1g} contribution to ΔE_{orb} is 64.7% of the total covalent interactions. The remaining orbital contributions are much smaller (< 11%). This is an example how qualitative arguments that have been put forward in the past can now be expressed in a quantitative form.

A somewhat surprising result came from the comparison of the bonding analysis of $FeCp_2$ with $Fe(\eta^5\text{-}N_5)_2$. Table 11 shows that the breakdown of the attractive $Fe^{2+}–(\eta^5\text{-}N_5^-)_2$ interactions into electrostatic (51.8%) and covalent (48.2%) contributions yields nearly the

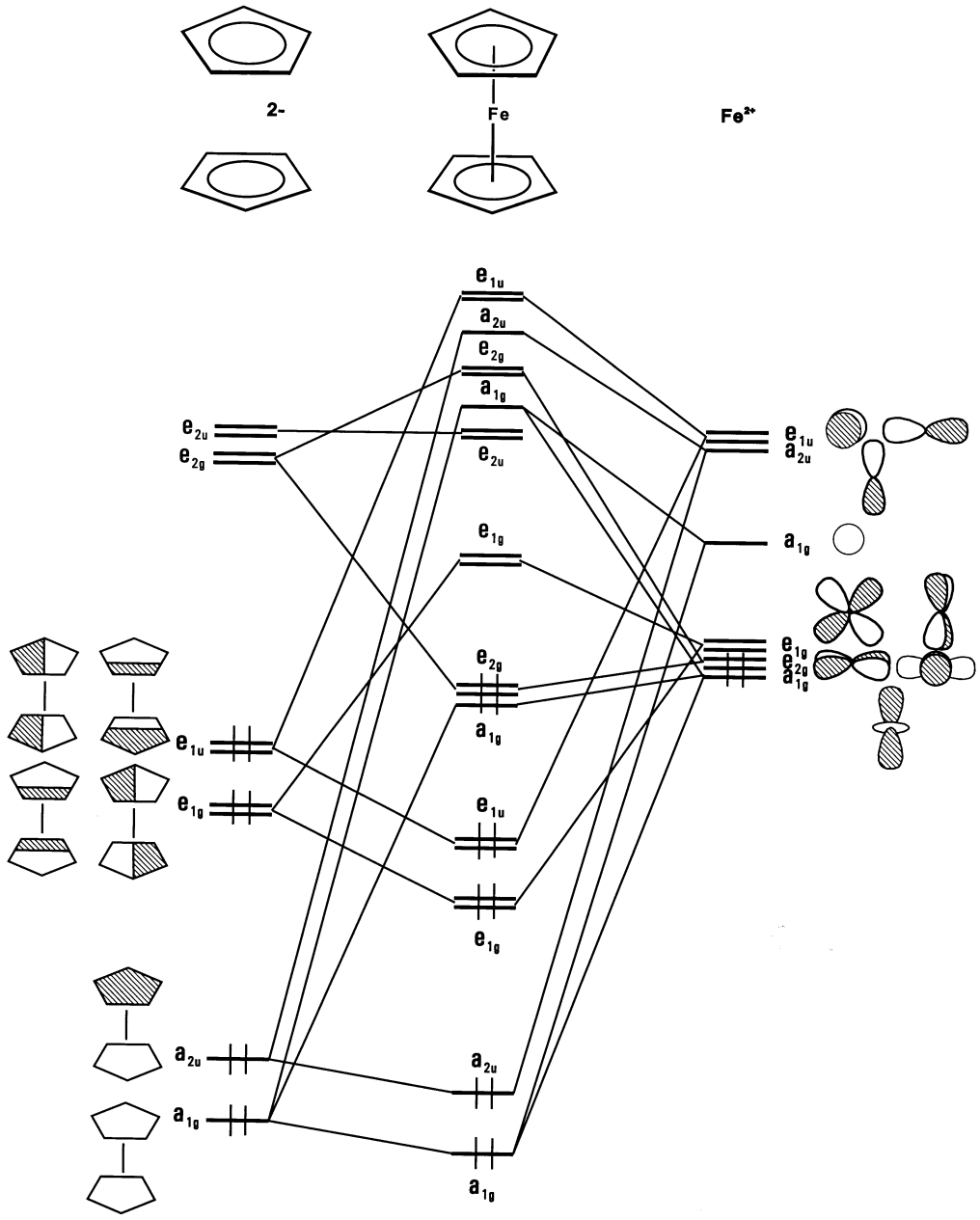

Fig. 14. MO correlation diagram for the interactions between Fe^{2+} and five-membered cyclic ligands cyc-E_5^- in (D_{5d}) Fe(η^5-E_5)$_2$ (E = CH, N).

same composition as in ferrocene. This means that the nature of the bonding in the two compounds is essentially the same. Examination of the different orbital terms shows that the (e_{1g})cyc-$N_5^- \rightarrow Fe^{2+}$ donation gives 65.5% of the total ΔE_{orb} term which is also very similar to the results for $FeCp_2$.

We investigated also the structures of the valence isoelectronic ferrocene analogues with one or two heterocyclic ligands, i.e. Fe(η^5-E_5)$_2$ and FeCp(η^5-E_5) (E = N–Sb). In order to investigate the changes in the bonding situation we analyzed the interaction energies between one η^5-E_5^- ligand and the Fe(η^5-E_5)$^+$ fragment. Fig. 15 gives the qualitative MO correlation diagram. Because the symmetry of the Fe(η^5-E_5)$^+$ fragment is C_{5v}, there are only contributions by orbitals which have a_1, e_1 and e_2 symmetry. There are no orbitals which have a_2 symmetry. The results of the energy analysis of the homoleptic complexes are given in Table 12.

A comparison of the data in Table 12 with those of Table 11 shows that the nature of the interactions between Fe(η^5-E_5)$^+$ and (η^5-E_5)$^-$ (E = CH, N) is very similar to the bonding between Fe^{2+} and $(Cp^-)_2$ and (η^5-N_5^-)$_2$ in ferrocene and iron bispentazole, respectively. The data show that the bonding in the heavier analogues Fe(η^5-E_5)$_2$ (E = P–Sb) is also not very

Table 11
Energy decomposition analysis of $Fe(Cp)_2$ and $Fe(N_5)_2$ at BP86/TZP (kcal mol^{-1}) [a,b]

	$Fe(C_5H_5)_2$	$Fe(N_5)_2$
ΔE_{int}	−893.3	−706.7
ΔE_{Pauli}	272.2	244.0
ΔE_{elstat}	−598.0 (51.3%) [c]	−492.6 (51.8%) [c]
ΔE_{orb}	−567.5 (48.7%) [c]	−458.1 (48.2%) [c]
ΔE (A_{1g})	−48.5 (8.5%) [d]	−40.6 (8.1%) [d]
ΔE (A_{2g})	0.0	0.0
ΔE (E_{1g})	−367.2 (64.7%) [d]	−285.4 (65.5%) [d]
ΔE (E_{2g})	−46.1 (8.1%) [d]	−44.7 (8.0%) [d]
ΔE (A_{1u})	0.0	0.0
ΔE (A_2)	−28.2 (5.0%) [d]	−22.3 (4.8%) [d]
ΔE (E_{1u})	−61.1 (10.8%) [d]	−44.5 (10.6%) [d]
ΔE (E_{2u})	−16.4 (2.9%) [d]	−20.6 (2.9%) [d]

[a] Taken from Ref. [43].
[b] $Fe^{2+}(t_{2g}^6) + 2L^-$.
[c] Percentage of attractive interactions $\Delta E_{elstat} + \Delta E_{orb}$.
[d] Percentage of orbital interactions ΔE_{orb}.

different from the bonding interactions in $FeCp_2$ and $Fe(\eta^5\text{-}N_5)_2$. Note that the phosphorous complex has about the same absolute value for the total interaction energy ΔE_{orb} (−199.5 kcal mol^{-1}) as the nitrogen complex (−198.0 kcal mol^{-1}) while the ΔE_{int} term of the heavier analogues has smaller values. The orbital interactions in the homocyclic and heterocyclic complexes $Fe(\eta^5\text{-}E_5)_2$ (E = CH–Sb) come mainly (63.8–69.4%) from the e_1 orbitals.

Table 13 gives the results of the energy analyses of the heteroleptic complexes $FeCp(\eta^5\text{-}E_5)$. Let us first discuss the results for the $CpFe^+$–$(\eta^5\text{-}E_5)^-$ interactions. The relative contributions of ΔE_{elstat} and ΔE_{orb} to the interaction energy are nearly the same as in the homoleptic complexes (Table 12). The $CpFe^+$–$(\eta^5\text{-}E_5)^-$ orbital interactions have a higher contribution from the e_2 orbitals and less contribution from the e_1 orbitals compared to $(\eta^5\text{-}E_5)Fe^+$–$(\eta^5\text{-}E_5)^-$. However, the most important difference of the bonding analysis of

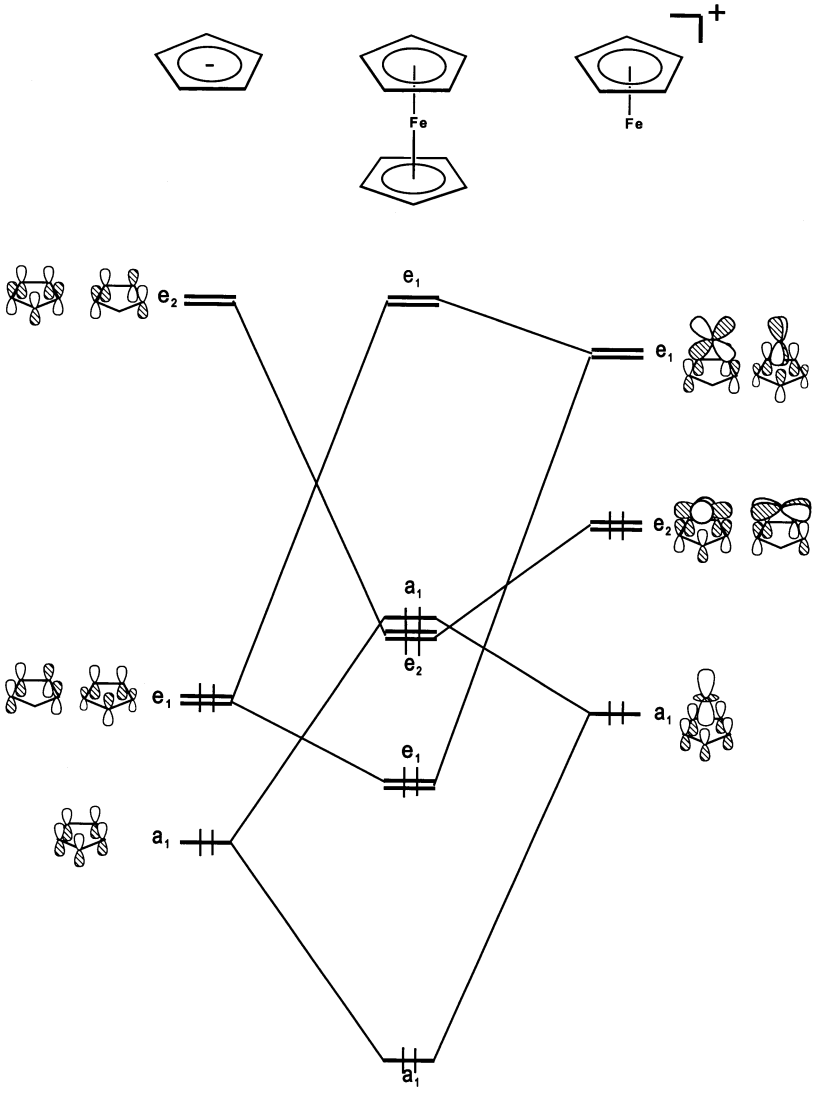

Fig. 15. MO correlation diagram for the interactions between a metal fragment $Fe(\eta^5\text{-}E_5)^+$ and a five-membered cyclic ligand E_5^- in (D_{5d}) $Fe(\eta^5\text{-}E_5)_2$ (E = CH, N–Sb).

Table 12
Energy decomposition analysis of $Fe(E_5)_2$ at BP86/TZP using the fragments $Fe(E_5)^+$ and E_5^- (kcal mol^{-1}) [c]

	E = CH	E = N	E = P	E = As	E = Sb
ΔE_{int}	−237.6	−198.0	−199.5	−183.8	−165.1
ΔE_{Pauli}	172.4	149.7	190.2	221.6	220.8
ΔE_{elstat} [a]	−238.5 (58.2%)	−184.3 (53.0%)	−207.3 (53.2%)	−223.1 (55.0%)	−205.1 (53.1%)
ΔE_{orb} [a]	−171.5 (41.8%)	−163.4 (47.0%)	−182.5 (46.8%)	−182.3 (45.0%)	−180.9 (46.9%)
$\Delta E(A_1)$ [b]	−25.0 (14.6%)	−22.4 (13.7%)	−28.1 (15.4%)	−29.1 (16.0%)	−35.7 (19.7%)
$\Delta E(A_2)$	0.0	0.0	0.0	0.0	0.0
$\Delta E(E_1)$ [b]	−109.3 (63.8%)	−106.1 (65.0%)	−120.7 (66.1%)	−123.7 (67.8%)	−125.6 (69.4%)
$\Delta E(E_2)$ [b]	−37.1 (21.6%)	−34.9 (21.3%)	−33.7 (18.5%)	−29.6 (16.2%)	−19.6 (10.8%)
ΔE_{prep}	2.8	13.1	28.0	23.3	46.3
ΔE ($= -D_e$)	−234.8	−184.9	−171.5	−160.5	−118.8

[a] The value in parentheses gives the percentage contribution to the total attractive interactions.
[b] The value in parentheses gives the percentage contribution to the total orbital interactions.
[c] Taken from Ref. [44].

the heterocyclic ligands between homoleptic and heteroleptic complexes is found for the total interaction energy ΔE_{int}. Table 13 shows that the phosphorous complex $FeCp(\eta^5\text{-}P_5)$ has clearly the highest value for ΔE_{int} (−214.7 kcal mol^{-1}). This is a higher value than in $Fe(\eta^5\text{-}P_5)_2$ (−199.5 kcal mol^{-1}). The calculations indicate that for the nitrogen analogues the bonding interactions in the heteroleptic complex $FeCp(\eta^5\text{-}N_5)$ are weaker (−164.5 kcal mol^{-1}) than in the homoleptic species $Fe(\eta^5\text{-}P_5)_2$ (−198.0 kcal mol^{-1}). The energy analysis suggests that the Cp ligand in $FeCp(\eta^5\text{-}E_5)$ weakens the Fe–$(\eta^5\text{-}E_5)$ bond with respect to $Fe(\eta^5\text{-}E_5)_2$ when E = N while it strengthens the bond when E = P, As, Sb. The calculated values of the energy contributions given in Tables 12 and 13 show that the weakening of the Fe–$(\eta^5\text{-}N_5)$ interactions in $FeCp(\eta^5\text{-}N_5)$ comes mainly from ΔE_{orb} while the stronger Fe–$(\eta^5\text{-}E_5)$ interactions (E = P–Sb) in the heteroleptic species come mainly from the increase of ΔE_{elstat}. The calculated changes for the Fe–Cp interactions in $FeCp(\eta^5\text{-}E_5)$ (Table 13) compared with $FeCp_2$ (Table 12) concur with the trend of the Fe–$(\eta^5\text{-}E_5)$ interactions. The data show that the Fe^+–$(Cp)^-$ interactions in $FeCp(\eta^5\text{-}N_5)$ (−298.6 kcal mol^{-1}) are much more attractive than in $FeCp_2$ while the ΔE_{int} values in the heavier $FeCp(\eta^5\text{-}E_5)$ (E = P–Sb) are smaller than in ferrocene.

Table 13
Energy decomposition analysis of $FeCp(E_5)$ at BP86/TZP using the fragments $FeCp^+ + E_5^-$ and $FeE_5^+ + Cp^-$ (kcal mol^{-1}) [c]

	$FeCp^+ + E_5^-$				$FeE_5^+ + Cp^-$			
	E = N	E = P	E = As	E = Sb	E = N	E = P	E = As	E = Sb
ΔE_{int}	−164.5	−214.7	−202.3	−186.3	−298.6	−232.3	−228.1	−223.1
ΔE_{Pauli}	151.1	195.3	152.0	128.3	179.5	222.0	241.4	267.8
ΔE_{elstat} [a]	−177.2 (56.1%)	−223.3 (54.5%)	−196.6 (55.5%)	−165.2 (52.5%)	−257.8 (53.9%)	−255.7 (56.3%)	−265.3 (56.5%)	−278.3 (56.7%)
ΔE_{orb} [a]	−138.5 (43.9%)	−186.7 (45.5%)	−157.7 (44.5%)	−149.3 (47.5%)	−220.3 (46.1%)	−198.6 (43.7%)	−204.1 (43.5%)	−212.6 (43.3%)
$\Delta E(A_1)$ [b]	−18.9 (13.7%)	−25.3 (13.6%)	−23.6 (15.0%)	−32.6 (21.8%)	−28.9 (13.1%)	−30.4 (15.3%)	−33.0 (16.2%)	−35.3 (16.6%)
$\Delta E(A_2)$	0.0	0.0	0.0	0.0	0.0	0.0	0.0	0.0
$\Delta E(E_1)$ [b]	−72.5 (52.3%)	−98.4 (52.7%)	−89.2 (56.5%)	−88.8 (59.5%)	−159.2 (72.3%)	−144.9 (73.0%)	−144.6 (70.8%)	−150.2 (70.6%)
$\Delta E(E_2)$ [b]	−47.1 (34.0%)	−63.0 (33.7%)	−45.0 (28.5%)	−27.9 (18.7%)	−32.2 (14.6%)	−23.3 (11.7%)	−26.5 (13.0%)	−27.2 (12.8%)
ΔE_{prep}	6.2	5.3	4.4	4.1	9.9	11.9	14.5	32.5
ΔE ($= -D_e$)	−158.3	−209.4	−197.9	−182.2	−288.7	−220.4	−213.6	−190.6

[a] The values in parentheses give the percentage contribution to the total attractive interactions.
[b] The values in parentheses give the percentage contribution to the total orbital interactions.
[c] Taken from Ref. [44].

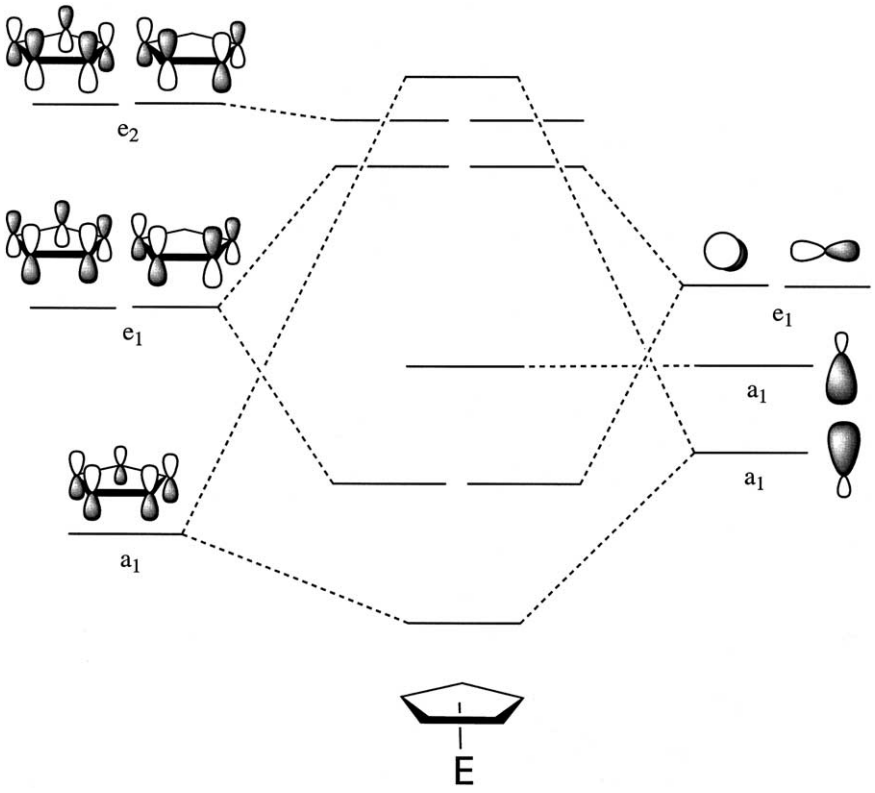

Fig. 16. MO correlation diagram for the interactions between a main group atomic ion E^+ and a Cp^- ligand in (C_{5v}) ECp.

8. Main group metallocenes ECp_2 (E = Be–Ba, Zn, Si–Pb) and ECp (E = Li–Cs, B–Tl)

The bonding situation in the ubiquitous metallococene complexes ECp_2 has also been studied by us for main group elements E where E is a Group-2 (Be–Ba) or -14 element (Si–Pb) or Zn. A comparison of the energy analysis with the results of ferrocene should give insight into the difference between the E–Cp_2 bonding of a transition metal and main group elements. We also investigated the metal–Cp bonding in the 'half sandwich' complexes ECp of Groups 1 (Li–Cs) and 13 (B–Tl) [46].

We first discuss the results of the half sandwich metallocenes ECp. Fig. 16 displays the orbital correlation diagram which is generally used for a qualitative bonding analysis [47]. There are only (σ)a_1- and (π)e_1-orbital interactions because the main group elements have no valence orbital that has e_2 symmetry. Tables 14 and 15 gives the results of the energy decomposition analysis between E^+ and Cp^-.

It has previously been suggested that the E–Cp bonding of the s-block elements (Groups 1 and 2) is mainly ionic while the p-block elements (Groups 13–18) should have significant covalent bonding [47]. The results in Table 14 show that the interaction energies in the alkaline complexes come mainly from electrostatic attraction which contribute between 80 and 90% of the total attraction. The largest covalent bonding is calculated for LiCp but it amounts to only 20.4%. The atomic partial charges also suggest substantial charge separation in ECp which means that the choice of the ionic fragments is not only convenient but also realistic. The covalent bonding comes mainly from the e_1 orbitals which contribute between 58 and 63% of the ΔE_{orb} values. The small values of the e_2 orbitals come from the relaxation of the ligand orbitals.

Table 15 shows that the strength of the covalent interactions in the Group-13 metallocenes ECp is significantly higher than in the alkaline analogues. The electrostatic and covalent bonding in BCp have nearly equal strength while the ΔE_{orb} term in the heavier analogues contributes between 28 and 35% of the total attraction. Note that the atomic partial charge at boron (+0.18) does not correlate with the substantial electrostatic character of the metal–ligand bond. The a_1 contribution to the covalent bonding in Group-13 metallocenes is significantly larger than in the Group-1 species, but the values of the e_1 orbitals are still larger than the a_1 values.

Next we turn to the metallocenes ECp_2 of Group-2 (E = Be–Ba) and -14 (E = Si–Pb). We did not analyze the bonding in the carbon analog CCp_2 because theoretical studies have shown that carbocene prefers a classical dicyclopentadienylcarbene structure and thus, a discussion in terms of a donor–acceptor metallocene

Table 14
Energy decomposition analysis of Group-1 metallocenes ECp (E = Li–Cs) at BP86/TZP (kcal mol^{-1}) [a]

	Li	Na	K	Rb	Cs
ΔE_{int}	−164.1	−138.0	−120.8	−113.9	−105.9
ΔE_{Pauli}	22.6	21.5	27.5	24.1	22.9
ΔE_{elstat}	−148.7 (79.6%) [b]	−138.0 (86.6%) [b]	−128.2 (86.4%) [b]	−121.0 (87.7%) [b]	−114.7 (89.1%) [b]
ΔE_{orb}	−38.1 (20.4%) [b]	−21.4 (13.4%) [b]	−20.1 (13.6%) [b]	−17.0 (12.3%) [b]	−14.1 (10.9%) [b]
$\Delta E(A_1)$	−9.6 (25.2%) [c]	−6.4 (29.9%) [c]	−5.2 (25.7%) [c]	−4.8 (28.4%) [c]	−4.2 (30.0%) [c]
$\Delta E(A_2)$	0.0	0.0	0.0	0.0	0.0
$\Delta E(E_1)$	−24.0 (63.0%) [c]	−12.3 (57.5%) [c]	−13.0 (64.4%) [c]	−10.5 (62.1%) [c]	−8.5 (60.7%) [c]
$\Delta E(E_2)$	−4.5 (11.8%) [c]	−2.7 (12.6%) [c]	−2.0 (9.9%) [c]	−1.6 (9.5%) [c]	−1.3 (9.3%) [c]
Atomic partial charges					
q(E)	+0.90	+0.91	+0.91	+0.94	+0.93

The symmetry point group is C_{5v}. NBO atomic partial charges q(E).
[a] Taken from Ref. [46].
[b] The values in parentheses give the percentage contribution to the total attractive interactions.
[c] The values in parentheses give the percentage contribution to the total orbital interactions.

Table 15
Energy decomposition analysis of Group-13 metallocenes ECp (E = B–Tl) at BP86/TZP (kcal mol^{-1}) [a]

	B	Al	Ga	In	Tl
ΔE_{int}	−256.0	−188.4	−181.2	−164.6	−155.0
ΔE_{Pauli}	202.2	118.1	97.1	81.6	67.2
ΔE_{elstat}	−226.1 (49.3%) [b]	−197.8 (64.6%) [b]	−183.5 (65.9%) [b]	−172.3 (70.0%) [b]	−160.0 (72.0%) [b]
ΔE_{orb}	−232.1 (50.7%) [b]	−108.6 (35.4%) [b]	−94.8 (34.1%) [b]	−73.9 (30.0%) [b]	−62.2 (28.0%) [b]
$\Delta E(A_1)$	−93.9 (40.4%) [c]	−47.9 (44.1%) [c]	−38.4 (40.5%) [c]	−29.7 (40.2%) [c]	−22.7 (36.5%) [c]
$\Delta E(A_2)$	0.0	0.0	0.0	0.0	0.0
$\Delta E(E_1)$	−130.1 (56.1%) [c]	−55.2 (50.8%) [c]	−51.9 (54.8%) [c]	−40.3 (54.5%) [c]	−36.3 (58.4%) [c]
$\Delta E(E_2)$	−8.10 (3.5%) [c]	−5.6 (5.1%) [c]	−4.5 (4.7%) [c]	−3.9 (5.3%) [c]	−3.2 (5.1%) [c]
Atomic partial charges					
q(E)	+0.18	+0.61	+0.57	+0.63	+0.62

The symmetry point group is C_{5v}. NBO atomic partial charges q(E).
[a] Taken from Ref. [46].
[b] The values in parentheses give the percentage contribution to the total attractive interactions.
[c] The values in parentheses give the percentage contribution to the total orbital interactions.

complex is not appropriate [48]. The bonding analysis was carried out for optimized geometries which have D_{5d} symmetry [46]. The calculations showed that some ECp_2 species have bent geometries where the bending angle X–E–X′ (X, X′ being the center of the Cp rings) is $<180^\circ$. The equilibrium geometries of $BeCp_2$ and $ZnCp_2$ have slipped sandwich structures where the Cp ligands are not always bonded in a η^5 fashion which is in agreement with experiment [46,47]. However, the energy differences between the D_{5d} form and the equilibrium structure is very small and therefore it seems justified to use the D_{5d} structure for the analysis of the bonding situation.

The qualitative orbital correlation diagram for the interaction between E^{2+} and $(Cp^-)_2$ in D_{5d} symmetry is displayed in Fig. 17. The valence s and p orbitals of the main group atom E have a_{1g}(s), $a_{2u}(p_\sigma)$ and $e_{1u}(p_\pi)$ symmetry. There is no s or p valence orbital of E which can mix with the e_{1g}-orbital of the ligands. For reasons which are given below we do show the higher lying empty d orbitals of E which are generally considered to be polarization functions but not true valence functions. Table 16 gives the results of the energy partitioning analysis of the Group-2 complexes ECp_2 (E = Be–Ba) and $ZnCp_2$.

The calculations suggest that the E^{2+}–$(Cp^-)_2$ bonding in the earth alkaline metallocenes is mainly ionic except in beryllocene which has a significant covalent character. The value for ΔE_{orb} gives 41% of the attractive interactions (Table 16). The covalent contributions in the heavier analogues are between 17 and 28% of the attractive interactions. The metal–ligand bonding in zincocene is ca. 2/3 electrostatic and ca. 1/3 covalent. The dominant contributions to the orbital interactions in beryllocene come from the e_{1u} orbitals (39.8%). The interactions of the a_{1g} and a_{2u} orbitals have

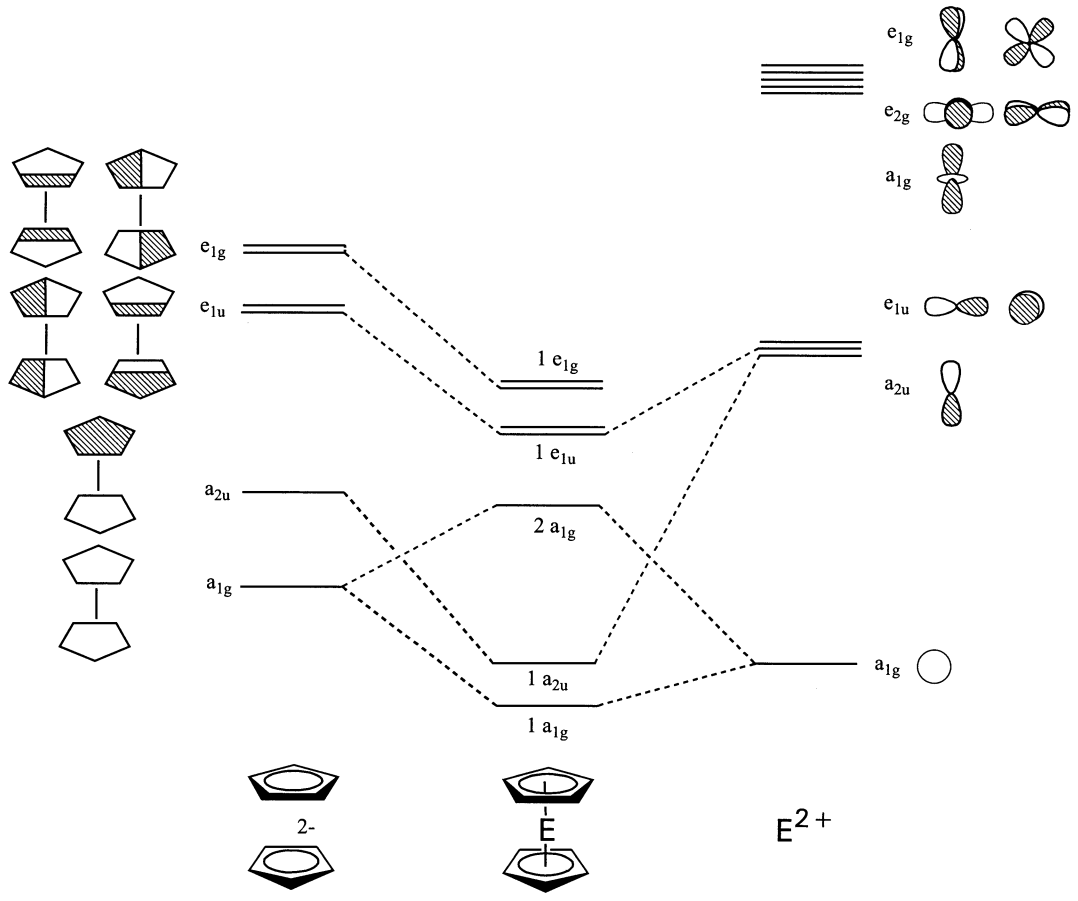

Fig. 17. MO correlation diagram for the interactions between a main group atomic ion E^{2+} and two Cp^- ligands in (D_{5d}) ECp_2.

Table 16
Energy decomposition analysis of Group-2 metallocenes ECp_2 (E = Be–Ba) and $ZnCp_2$ at BP86/TZP (kcal mol^{-1}) [a]

	Be	Mg	Ca	Sr	Ba	Zn
ΔE_{int}	−780.9	−636.7	−549.0	−504.5	−461.0	−707.9
ΔE_{Pauli}	35.9	52.7	73.6	66.5	62.2	85.5
ΔE_{elstat}	−483.2 (59.2%) [b]	−493.6 (71.6%) [b]	−477.9 (76.8%) [b]	−458.3 (80.3%) [b]	−437.0 (83.5%) [b]	−533.6 (67.3%) [b]
ΔE_{orb}	−333.6 (40.8%) [b]	−195.8 (28.4%) [b]	−144.7 (23.2%) [b]	−112.7 (19.7%) [b]	−86.2 (16.5%) [b]	−259.8 (32.7%) [b]
$\Delta E(A_{1g})$	−58.6 (17.6%) [c]	−38.9 (19.9%) [c]	−21.5 (14.9%) [c]	−18.2 (16.1%) [c]	−13.8 (16.0%) [c]	−80.6 (31.0%) [c]
$\Delta E(A_{2g})$	0.0	0.0	0.0	0.0	0.0	0.0
$\Delta E(E_{1g})$	−53.5 (16.0%) [c]	−47.6 (24.3%) [c]	−63.0 (43.5%) [c]	−45.5 (40.4%) [c]	−32.0 (37.1%) [c]	−39.1 (15.0%) [c]
$\Delta E(E_{2g})$	−15.8 (4.7%) [c]	−12.5 (6.4%) [c]	−9.1 (6.3%) [c]	−7.1 (6.3%) [c]	−5.5 (6.4%) [c]	−15.1 (5.8%) [c]
$\Delta E(A_{1u})$	0.0	0.0	0.0	0.0	0.0	0.0
$\Delta E(A_{2u})$	−58.9 (17.6%) [c]	−26.6 (13.6%) [c]	−13.0 (9.0%) [c]	−10.0 (8.9%) [c]	−7.9 (9.2%) [c]	−35.5 (13.7%) [c]
$\Delta E(E_{1u})$	−132.8 (39.8%) [c]	−59.0 (30.1%) [c]	−29.6 (20.5%) [c]	−24.7 (21.9%) [c]	−21.2 (24.6%) [c]	−78.4 (30.2%) [c]
$\Delta E(E_{2u})$	−14.1 (4.2%) [c]	−11.3 (5.8%) [c]	−8.5 (5.9%) [c]	−7.2 (6.4%) [c]	−5.9 (6.8%) [c]	−11.2 (4.3%) [c]
Atomic partial charges						
q(E)	+1.68	+1.74	+1.72	+1.77	+1.77	+1.60

The symmetry point group is D_{5d}. NBO atomic partial charges q(E).
[a] Taken from Ref. [46].
[b] The values in parentheses give the percentage contribution to the total attractive interactions.
[c] The values in parentheses give the percentage contribution to the total orbital interactions.

the same strength (17.6%). The relaxation energy of the e_{1g} orbitals add another 16% to the ΔE_{orb} term. The relaxation of the e_{1g} ligand orbitals is further supported by mixing with the e_{1g}(d) orbitals of E^{2+} (Fig. 17). A somewhat surprising result of the energy analysis of the heavier earth alkaline complexes $MgCp_2$–$BaCp_2$ was

the strength of the e_{1g}-orbital contribution to ΔE_{orb}. Table 16 shows that the latter interaction increases when E is a heavier element, and that the value for the e_{1g}-orbital contributions becomes even the largest one for $CaCp_2$, $SrCp_2$ and $BaCp_2$. We do not think, however, that the relatively high value for the e_{1g}-orbital contributions should be interpreted as genuine d-orbital participation in covalent E–Cp bonding. We want to point out that the total covalent contributions to the bonding in $MgCp_2$–$BaCp_2$ is rather small. The absolute values of the e_{1g}-orbital contributions in all earth alkaline metallocenes inclusive $BeCp_2$ remain rather constant which indicates that a similar effect may be responsible for the energy lowering. The e_{1g}-orbital is the HOMO of the complexes and thus, it is the most polarizable occupied MO. The empty d functions of atom E are optimally shaped for mixing with the e_{1g} ligand orbital and thus, they will be used for the relaxation of the MO throughout the whole series ECp_2 (E = Be–Ba). The orbital interactions in zincocene come mainly from the a_{1g} (31.0%) and e_{1u} (30.2%) MOs.

Table 17
Energy decomposition analysis of Group-14 metallocenes ECp_2 (E = Si, Ge, Sn, Pb) at BP86/TZP (kcal mol^{-1}) [a]

	Si	Ge	Sn	Pb
ΔE_{int}	−685.4	−661.4	−601.4	−577.2
ΔE_{Pauli}	120.4	108.7	101.6	91.3
ΔE_{elstat}	−506.7 (62.9%) [b]	−501.3 (65.1%) [b]	−490.0 (69.7%) [b]	−480.2 (71.8%) [b]
ΔE_{orb}	−299.1 (37.1%) [b]	−268.7 (34.9%) [b]	−213.0 (30.3%) [b]	−188.3 (28.2%) [b]
$\Delta E(A_{1g})$	−16.6 (5.6%) [c]	−13.2 (4.9%) [c]	−12.2 (5.7%) [c]	−10.3 (5.5%) [c]
$\Delta E(A_{2g})$	0.0	0.0	0.0	0.0
$\Delta E(E_{1g})$	−48.9 (16.3%) [c]	−37.7 (14.0%) [c]	−28.9 (13.6%) [c]	−24.9 (13.2%) [c]
$\Delta E(E_{2g})$	−9.7 (3.2%) [c]	−9.0 (3.3%) [c]	−7.8 (3.6%) [c]	−7.3 (3.9%) [c]
$\Delta E(A_{1u})$	0.0	0.0	0.0	0.0
$\Delta E(A_{2u})$	−58.7 (19.6%) [c]	−54.2 (20.2%) [c]	−41.5 (19.5%) [c]	−36.3 (19.3%) [c]
$\Delta E(E_{1u})$	−156.4 (52.3%) [c]	−146.5 (54.5%) [c]	−115.2 (54.1%) [c]	−102.7 (54.5%) [c]
$\Delta E(E_{2u})$	−8.8 (2.9%) [c]	−8.2 (3.1%) [c]	−7.5 (3.5%) [c]	−6.8 (3.6%) [c]
Atomic partial charges				
q(E)	+0.80	+0.86	+0.98	+0.99

The symmetry point group is D_{5d}. NBO atomic partial charges q(E).
[a] Taken from Ref. [46].
[b] The values in parentheses give the percentage contribution to the total attractive interactions.
[c] The values in parentheses give the percentage contribution to the total orbital interactions.

Table 17 gives the results of the energy partitioning analysis of the Group-14 metallocenes $SiCp_2$–$PbCp_2$. The covalent contributions to the bonding are larger than in the earth alkaline metallocenes (Table 16) but the electrostatic interactions are still clearly more important than the covalent attractions. The ΔE_{orb} term provides between 28 and 37% of the total attraction. The contributions of the orbitals with different symmetry are remarkably constant from $SiCp_2$ to $PbCp_2$ (Table 17). Half of the value of the ΔE_{orb} term comes from the e_{1u} orbitals while ca. 20% comes from the a_{2u} orbitals. Note that the contribution of the e_{1g} term remains small compared with the strong increase for the heavier earth alkaline metallocenes. This is a hint that the large contributions in the latter complexes are indeed caused by polarization and not by covalent bonding. The polarization functions of the earth alkaline elements are much more diffuse than those of the Group-14 elements and therefore, they have a larger overlap with the ligand orbitals.

Table 18 gives the contributions of ΔE_{Pauli}, ΔE_{elstat} and ΔE_{orb} to the total interaction energy ΔE_{int} for those ECp_2 complexes which have a bent equilibrium geometry. It becomes obvious that the values of the three energy terms in the D_{5d} structures and in the lowest energy form are not very different from each other. Thus, the conclusions about the nature of the metal–ligand bonding in terms of covalent and electrostatic interactions in the D_{5d} form of the metallocenes holds also for the equilibrium geometries.

9. Summary and conclusion

The results of the energy partitioning analysis of a variety of donor–acceptor complexes of transition

Table 18
Energy decomposition analysis of the ECp_2 at the bent equilibrium geometry (E = Sr, Ba, Si, Ge, Sn, Pb, Zn) at BP86/TZP (kcal mol^{-1}) [a]

	Sr (C_1)	Ba (C_s)	Si (C_2)	Ge (C_s)	Sn (C_s)	Pb (C_1)	Zn (C_s)
ΔE_{int}	−505.6	−461.4	−691.9	−663.2	−604.0	−578.0	−720.0
ΔE_{Pauli}	79.6	87.6	153.1	119.4	110.1	94.5	113.3
ΔE_{elstat}	−466.8 (79.7%) [b]	−452.7 (82.4%) [b]	−513.2 (60.7%) [b]	−504.0 (64.4%) [b]	−492.5 (69.0%) [b]	−481.6 (71.7%) [b]	−553.1 (66.4%) [b]
ΔE_{orb}	−118.4 (20.3%) [b]	−96.3 (17.6%) [b]	−331.8 (39.3%) [b]	−278.7 (35.6%) [b]	−221.6 (31.0%) [b]	−190.8 (28.3%) [b]	−280.2 (33.6%) [b]

[a] Taken from Ref. [46].
[b] The values in parentheses give the percentage contribution to the total attractive interactions.

metals and main-group elements demonstrates that it is possible to examine the nature of a chemical bond not only qualitatively but quantitatively [53]. This is possible for two reasons. One reason is that the geometries and energies of heavy-atom molecules can be accurately calculated with modern quantum chemical methods. The second reason is that the interaction energies between atoms or fragments can be partitioned in a plausible way such that the resulting energy terms are well defined and can be interpreted and identified with elementary physical concepts. The speculative discussions whether a chemical bond is more electrostatic or more covalent which often leads to controversies that cannot be resolved because of vague definitions and questionable correlations with experimental data can now be addressed by precise answers. However, the quantitative statements about the electrostatic and covalent contributions to a bond and the strength of the orbital contributions having different symmetry should not be mistaken for a determination of these factors in the sense of a physical measurement. Nature does not distinguish between covalent and electrostatic interactions and there is no way to determine ΔE_{orb} or ΔE_{elstat} like a bond length or a bond dissociation energy. The advantage of performing an energy partitioning analysis as described here is the establishment of a plausible and well defined ordering scheme which makes it possible to compare chemical bonds quantitatively. We want to point out that the interpretation of the nature of the chemical bond which is presented generally agrees quite well with 'chemical intuition' and previous assumptions which were based on qualitative arguments. Thus, the results of the energy partitioning analysis do not yield a completely different picture of the chemical bond compared with previous suggestions. This should be an advantage when it comes to the question whether the quantitative interpretation of the chemical bond which is presented here becomes accepted by the majority of chemists.

Finally, we should mention that the energy partitioning scheme which is used in our work can also be applied to analyze the nature of the chemical bond between open-shell fragments. It is possible to investigate the nature of covalent bonds which break homolytically and not heterolytically as in donor–acceptor complexes. It is our goal to extend systematically the energy partitioning analysis to all types of chemical bonds. We will report our progress in future publications.

Acknowledgements

We want to thank both reviewers who forced us with their thoughtful comments, questions and suggestions to state our arguments more precisely and on this way helped to improve the paper. The work was supported by the Deutsche Forschungsgemeinschaft and by the Fonds der Chemischen Industrie. G.F. thanks Matthias Bickelhaupt and Evert-Jan Baerends for helpful comments and stimulating discussions. V.M.R. thanks the Secretaría de Estado de Educación y Universidades (MECD-Spain) for support via grant EX-01-09396368V. Excellent service by the Hochschulrechenzentrum of the Philipps-Universität Marburg is gratefully acknowledged. Additional computer time was provided by the HLRS Stuttgart and HHLRZ Darmstadt.

References

[1] R.G. Pearson, Introduction to Hard and Soft Acids and Bases, Dowden, Hutchinson, Ross, Stroudsburg PA, 1973.
[2] R.J. Gillespie, I. Hargittai, The VSEPR Model of Molecular Geometry, Allyn & Bacon, Boston, 1991.
[3] R.B. Woodward, R. Hoffmann, The Conservation of Orbital Symmetry, Verlag Chemie, Weinheim, 1970.
[4] (a) K. Fukui, Acc. Chem. Res. 4 (1971) 57;
(b) I. Fleming, Frontier Orbitals and Organic Chemical Reactions, Wiley, New York, 1976.
[5] L. Pauling, The Nature of the Chemical Bond, 3rd ed., Cornell University Press, Ithaka, New York, 1960.
[6] A.Y. Timoshkin, G. Frenking, J. Am. Chem. Soc. 124 (2002) 7240.
[7] We want to remind the reader that π bonding is a symmetry term which is not synonymous with double bonding. A molecule which belongs to a point group that has a mirror plane has always π orbitals but may not have a double bond as e.g. CH_4.
[8] J. Su, X.-W. Li, R.C. Crittendon, C.F. Campana, G.H. Robinson, Organometallics 16 (1997) 4511.
[9] J. Su, X.-W. Li, R.C. Crittendon, G.H. Robinson, J. Am. Chem. Soc. 119 (1997) 5471.
[10] (a) F.A. Cotton, X. Feng, Organometallics 17 (1998) 128;
(b) C. Boehme, G. Frenking, Chem. Eur. J. 5 (1999) 2184;
(c) J. Uddin, C. Boehme, G. Frenking, Organometallics 19 (2000) 571;
(d) C. Boehme, J. Uddin, G. Frenking, Coord. Chem. Rev. 197 (2000) 249.
[11] (a) F.A. Cotton, A.H. Cowley, X. Feng, J. Am. Chem. Soc. 120 (1998) 1795;
(b) T.L. Allen, W.H. Fink, P.P. Power, J. Chem. Soc. Dalton Trans. (2000) 407.
[12] (a) F.M. Bickelhaupt, E.J. Baerends, in: K.B. Lipkowitz, D.B. Boyd (Eds.), Rev. Comput. Chem, vol. 15, Wiley-VCH, New York, 2000, p. 1;
(b) G. te Velde, F.M. Bickelhaupt, E.J. Baerends, S.J.A. van Gisbergen, C. Fonseca Guerra, J.G. Snijders, T. Ziegler, J. Comput. Chem. 22 (2001) 931.
[13] (a) K. Morokuma, J. Chem. Phys. 55 (1971) 1236;
(b) K. Kitaura, K. Morokuma, Int. J. Quantum Chem. 10 (1976) 325.
[14] T. Ziegler, A. Rauk, Theor. Chim. Acta 46 (1977) 1.
[15] (a) A.D. Becke, J. Chem. Phys. 98 (1993) 5648;
(b) C. Lee, W. Yang, R.G. Parr, Phys. Rev. B 37 (1988) 785;
(c) P.J. Stevens, F.J. Devlin, C.F. Chablowski, M.J. Frisch, J. Phys. Chem. 98 (1994) 11623.
[16] (a) A.D. Becke, Phys. Rev. A 38 (1988) 3098;
(b) J.P. Perdew, Phys. Rev. B 33 (1986) 8822.
[17] (a) C. Chang, M. Pelissier, Ph. Durand, Phys. Scr. 34 (1986) 394;
(b) J.-L. Heully, I. Lindgren, E. Lindroth, S. Lundquist, A.-M.

Martensson-Pendrill, J. Phys. B 19 (1986) 2799;
(c) E. van Lenthe, E.J. Baerends, J.G. Snijders, J. Chem. Phys. 99 (1993) 4597;
(d) E. van Lenthe, E.J. Baerends, J.G. Snijders, J. Chem. Phys. 105 (1996) 6505;
(e) E. van Lenthe, R. van Leeuwen, E.J. Baerends, J.G. Snijders, Int. J. Quantum Chem. 57 (1996) 281.

[18] Selected examples: (a) T. Ziegler, V. Tschinke, A.D. Becke, J. Am. Chem. Soc. 109 (1987) 1351;
(b) T. Ziegler, V. Tschinke, C. Ursenbach, J. Am. Chem. Soc. 109 (1987) 4825;
(c) J. Li, G. Schreckenbach, T. Ziegler, J. Am. Chem. Soc. 117 (1995) 486;
(d) A.W. Ehlers, E.J. Baerends, F.M. Bickelhaupt, U. Radius, Chem. Eur. J. 4 (1998) 210.

[19] (a) M.J.S. Dewar, Bull. Soc. Chim. Fr. 18 (1951) C79;
(b) For a historic perspective of Dewar's paper and its influence of bonding models see the special issue of J. Organomet. Chem., 635.

[20] (a) C.W. Bauschlicher, P.S. Bagus, J. Chem. Phys. 81 (1984) 5889;
(b) C.W. Bauschlicher, L.G.M. Petterson, P.E.M. Siegbahn, J. Chem. Phys. 87 (1987) 2129;
(c) C.W. Bauschlicher, S.R. Langhoff, L.A. Barnes, Chem. Phys. 129 (1989) 431;
(d) C.W. Bauschlicher, J. Chem. Phys. 84 (1986) 260;
(e) C.W. Bauschlicher, P.S. Bagus, C.J. Nelin, B.O. Roos, Chem. Phys. 85 (1986) 354;
(f) L.A. Barnes, M. Rosi, C.W. Bauschlicher, J. Chem. Phys. 94 (1991) 2031;
(g) L.A. Barnes, M. Rosi, C.W. Bauschlicher, J. Chem. Phys. 93 (1990) 609;
(h) L.A. Barnes, C.W. Bauschlicher, J. Chem. Phys. 91 (1989) 314.;
(i) M.R.A. Blomberg, U.B. Brandemark, P.E.M. Siegbahn, J. Wennerberg, C.W. Bauschlicher, J. Am. Chem. Soc. 110 (1988) 6650;
(j) M.B. Hall, R.F. Fenske, Inorg. Chem. 11 (1972) 1620;
(k) P.E. Sherwood, M.B. Hall, Inorg. Chem. 18 (1979) 2325;
(l) P.E. Sherwood, M.B. Hall, Inorg. Chem. 19 (1980) 1805;
(m) R.L. Williamson, M.B. Hall, Int. J. Quantum Chem. 21S (1987) 503;
(n) I.H. Hillier, V.R. Saunders, Mol. Phys. 23 (1971) 1025;
(o) I.H. Hillier, V.R. Saunders, J. Chem. Soc. Chem. Commun. (1971) 642;
(p) P.C. Ford, I.H. Hillier, J. Chem. Phys. 80 (1984) 5664;
(q) P.C. Ford, I.H. Hillier, S.A. Pope, M.F. Guest, Chem. Phys. Lett. 102 (1983) 555;
(r) G. Cooper, J.C. Green, M.P. Payne, B.R. Dobson, I.H. Hillier, Chem. Phys. Lett. 125 (1986) 97;
(s) G. Cooper, J.C. Green, M.P. Payne, B.R. Dobson, I.H. Hillier, M. Vincent, M. Rosi, J. Chem. Soc. Chem. Commun. (1986) 438;
(t) D. Moncrieff, P.C. Ford, I.H. Hillier, V.R. Saunders, J. Chem. Soc. Chem. Commun. (1983) 1108;
(u) S. Smith, I.H. Hillier, W. von Niessen, M.C. Guest, Chem. Phys. 135 (1989) 357;
(v) L.G. Vanquickenborne, J. Verhulst, J. Am. Chem. Soc. 109 (1987) 4825;
(w) K. Pierfoot, J. Verhulst, P. Verbeke, L.G. Vanquickenborne, Inorg. Chem. 28 (1989) 3059;
(x) S. Yamamoto, H. Kashiwagi, Chem. Phys. Lett. 205 (1993) 306;
(y) M.R.A. Blomberg, P.E.M. Siegbahn, T.L. Lee, A.P. Rendell, J.E. Rice, J. Chem. Phys. 95 (1991) 5898.

[21] (a) E.J. Baerends, A. Rozendaal, in: A. Veillard (Ed.), Quantum Chemistry: The Challenge of Transition Metals and Coordination Chemistry, D. Reidel Publishing Company, Dordrecht, 1986, p. 159;
(b) E.R. Davidson, K.L. Kunze, F.B.C. Machado, S.J. Chakravorty, Acc. Chem. Res. 26 (1993) 628;
(c) K.L. Kunze, E.R. Davidson, J. Phys. Chem. 96 (1992) 2129;
(d) F.B.C. Machado, E.R. Davidson, J. Phys. Chem. 97 (1993) 4397;
(e) J. Li, G. Schreckenbach, T. Ziegler, J. Am. Chem. Soc. 117 (1995) 486;
(f) S.-C. Chung, S. Krüger, S.Ph. Ruzankin, G. Pacchioni, N. Rösch, Chem. Phys. Lett. 248 (1996) 109.

[22] A charge decomposition analysis of positively and negatively charged carbonyl complexes was presented by: R.K. Szilagy, G. Frenking, Organometallics 16 (1997) 4807.

[23] A. Diefenbach, F.M. Bickelhaupt, G. Frenking, J. Am. Chem. Soc. 122 (2000) 6449.

[24] T.A. Albright, J.K. Burdett, M.H. Whangbo, Orbital Interactions in Chemistry, Wiley, New York, 1985.

[25] (a) T.K. Firman, C.R. Landis, J. Am. Chem. Soc. 120 (1998) 12650;
(b) C.A. Bayse, M.B. Hall, J. Am. Chem. Soc. 121 (1999) 1348.

[26] (a) J. Weiß, D. Stetzkamp, B. Nuber, R.A. Fischer, C. Boehme, G. Frenking, Angew. Chem. 109 (1997) 95;
(b) J. Weiß, D. Stetzkamp, B. Nuber, R.A. Fischer, C. Boehme, G. Frenking, Angew. Chem. Int. Ed. Engl. 36 (1997) 70.

[27] (a) H. Braunschweig, C. Kollann, U. Englert, Angew. Chem. 110 (1998) 3355;
(b) H. Braunschweig, C. Kollann, U. Englert, Angew. Chem. Int. Ed. Engl. 37 (1998) 3179.

[28] C. Boehme, J. Uddin, G. Frenking, Coord. Chem. Rev. 197 (2000) 249.

[29] (a) R.A. Fischer, M.M. Schulte, J. Weiss, L. Zsolnai, A. Jacobi, G. Huttner, G. Frenking, C. Boehme, S.F. Vyboishchikov, J. Am. Chem. Soc. 120 (1998) 1237;
(b) D. Weiss, T. Steinke, M. Winter, R.A. Fischer, N. Fröhlich, J. Uddin, G. Frenking, Organometallics 19 (2000) 4583;
(c) G. Frenking, J. Uddin, W. Uhl, M. Benter, S. Melle, W. Saak, Organometallics 18 (1999) 3778.

[30] An energy partitioning analysis was also published by other workers who did not identify the covalent and electrostatic contributions nor the σ and π bonding: C.L.B. Macdonald, A.H. Cowley, J. Am. Chem. Soc. 121 (1999) 12113.

[31] (a) J. Uddin, G. Frenking, J. Am. Chem. Soc. 123 (2001) 1683;
(b) M. Doerr, G. Frenking, Z. Allg. Anorg. Chem. 628 (2002) 843.

[32] A.E. Reed, L.A. Curtiss, F. Weinhold, Chem. Rev. 88 (1988) 899.

[33] Note that Table 5 gives the results of the equatorial isomers of $(CO)_4Fe–EMe$ because Table 6 gives the energy analysis of the equatorial $(EMe)_4Fe–EMe$ bond.

[34] Reviews: (a) P. Fantucci, Comments Inorg. Chem. 13 (1992) 241;
(b) P.B. Dias, M.E. Minas de Piedade, J.A. Martinho Simoes, Coord. Chem. Rev. 135/136 (1994) 738;
(c) E.C. Alyea, S. Song, Comments Inorg. Chem. 18 (1996) 145;
(d) E.C. Alyea, S. Song, Comments Inorg. Chem. 18 (1996) 189.

[35] F.A. Cotton, C.S. Kraihanzel, J. Am. Chem. Soc. 84 (1962) 4432.

[36] J.E. Huheey, E.A. Keiter, R.L. Keiter, Inorganic Chemistry: Principles and Structure of Reactivity, 4th ed., Harper Collins College Publishers, New York, 1993, p. 431.

[37] Y. Ruiz-Morales, T. Ziegler, J. Phys. Chem. Sect. A 102 (1998) 3970.

[38] G. Frenking, K. Wichmann, N. Fröhlich, J. Grobe, W. Golla, D. Le Van, B. Krebs, M. Läge, Organometallics 21 (2002) 2921.

[39] An energy partitioning analysis of phosphane complexes $(CO)_4FePR_3$ has also been reported in: Ó. Gonzáles-Blanco, V. Branchadell, Organometallics 16 (1997) 5556. However, the authors used only the frontier orbital interactions as σ and π contributions while the remaining orbital interactions were considered as residual stabilization E_{res}.

[40] In Ref. [38], we give also the results of a detailed charge partitioning of the complexes which supplement the energy analysis.
[41] C. Loschen, K. Voigt, J. Frunzke, A. Diefenbach, M. Diedenhofen, G. Frenking, Z. Allg. Anorg. Chem. 628 (2002) 1294.
[42] R.J. Gillespie, P.L.A. Popelier, Chemical Bonding and Molecular Geometry, Oxford University Press, New York, 2001.
[43] M. Lein, J. Frunzke, A. Timoshkin, G. Frenking, Chem. Eur. J. 7 (2001) 4155.
[44] J. Frunzke, M. Lein, G. Frenking, Organometallics 21 (2002) 3351.
[45] Ch. Elschenbroich, A. Salzer, Organometallics, 2nd ed., VCH, Weinheim, 1992.
[46] V.M. Rayón, G. Frenking, Chem. Eur. J., 8 (2002) 4693.
[47] Recent reviews: (a) O. Kwon, M.L. McKee, in: T.R. Cundari (Ed.), Computational Organometallic Chemistry, Marcel Dekker, New York, 2001, p. 397f;
(b) P. Jutzi, N. Burford, Chem. Rev. 99 (1999) 969;
(c) P. Jutzi, N. Burford, in: A. Togni, R.L. Haltermann (Eds.), Metallocenes, vol. 1, Wiley-VCH, New York, 1998, p. 3f.
[48] W.W. Schoeller, O. Friedrich, A. Sundermann, A. Rozhenko, Organometallics 18 (1999) 2099.
[49] A comparative analysis of the metal–ligand interactions of Group-13 ligands BR with isoelectronic CO, N_2, SiO and BO^- using the energy decomposition scheme was reported in Ref. 18d and in: (a) F.M. Bickelhaupt, U. Radius, A.W. Ehlers, R. Hoffmann, E.J. Baerends, New J. Chem. 22 (1998) 1;
(b) U. Radius, F.M. Bickelhaupt, A.W. Ehlers, N. Goldberg, R. Hoffmann, Inorg. Chem. 37 (1998) 1080.
[50] J. Cioslowski, in: P.v.R. Schleyer, N.L. Allinger, P.A. Kollmann, T. Clark, H.F. Schaefer, III, J. Gasteiger (Eds.), Encyclopedia of Computational Chemistry, vol. 2, Wiley, Chichester, 1998, p. 892.
[51] (a) R.F. Frey, E.R. Davidson, J. Chem. Phys. 90 (1989) 5555;
(b) S.M. Cybulski, S. Scheiner, Chem. Phys. Lett. 166 (1990) 57;
(c) M. Martinov, J. Cioslowski, Mol. Phys. 85 (1995) 121.
[52] Please note that the energy partitioning analysis of the $(CO)_5W$–CO bond gives a larger contribution by ΔE_{elstat} (53.6%) than by ΔE_{orb} (46.4%, Table 1) while the results for the $W–(CO)_6$ interactions show larger values for ΔE_{orb} (56.6%) than for ΔE_{elstat} (43.3%, Table 2). This is because the nature of the bond A–B depends on the atomic connectivity and electronic structure of the fragments A and B.
[53] Previous methods such as MO correlation diagrams have also been used in the past for a quantitative analysis of the chemical bonds. However, they were mainly based on methods such as EHT and the numbers are less meaningful than those which are reported here.